



27-29 October 2025

Progress towards high-density superconductor digital logic

Leonard M. Johnson

Quantum-Enabled Computation Group



DISTRIBUTION STATEMENT A. Approved for public release. Distribution is unlimited.

This material is based upon work supported by the Under Secretary of War for Research and Engineering under Air Force Contract No. FA8702-15-D-0001 or FA8702-25-D-B002. Any opinions, findings, conclusions or recommendations expressed in this material are those of the author(s) and do not necessarily reflect the views of the Under Secretary of War for Research and Engineering.

© 2025 Massachusetts Institute of Technology.

Delivered to the U.S. Government with Unlimited Rights, as defined in DFARS Part 252.227-7013 or 7014 (Feb 2014). Notwithstanding any copyright notice, U.S. Government rights in this work are defined by DFARS 252.227-7013 or DFARS 252.227-7014 as detailed above. Use of this work other than as specifically authorized by the U.S. Government may violate any copyrights that exist in this work.



MIT Lincoln Laboratory Quantum-Enabled Computation Group

Quantum-Enabled Computation Group

MIT Lincoln Laboratory



**Federally-funded research & development center
located in Lexington, Massachusetts**

~4500 employees

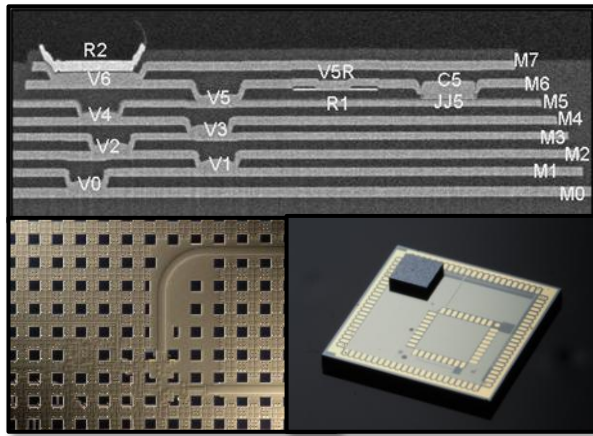




Quantum-Enabled Computation Group

Mission: Develop advanced hardware, systems, and algorithms that leverage quantized signals for transformative computational advantage

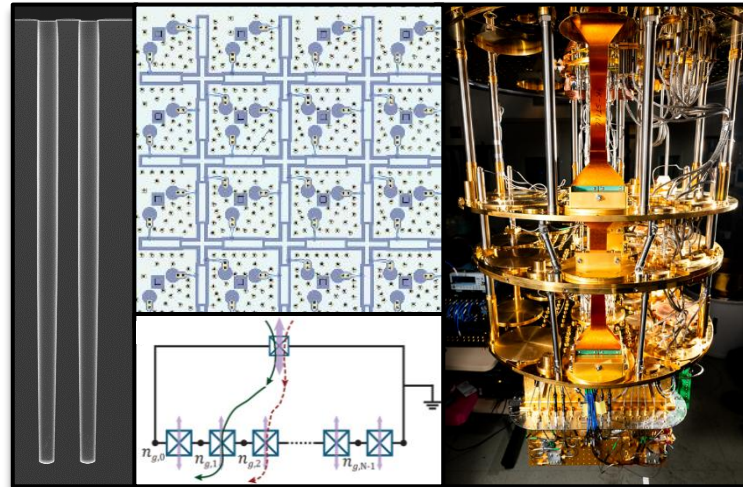
Superconductor Electronics (SCE)



- Demonstrating and validating efficient SCE supercomputing and processing concepts
- Enhancing SCE foundry capabilities to access new paradigms for cryogenic computing
- Enabling new sensing, detection, control, and digitization capabilities with SCE electronics

Demonstrate transformative capabilities in SCE platforms and applications

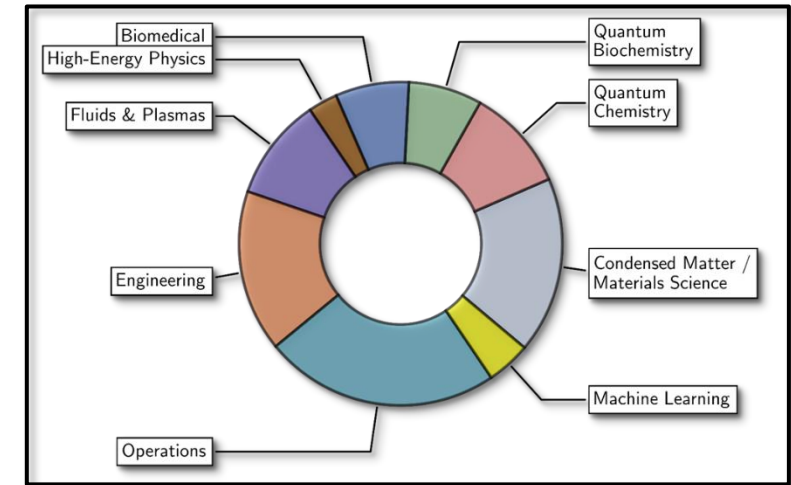
Superconducting Qubits (SCQ)



- Advancing fundamental science of SCQ devices
- Pathfinding for advanced integration & routing
- Building verification and validation protocols for quantum logic
- Accelerating fundamental research via SQUILL Foundry

Chart the path to useful quantum computation with superconducting devices

Quantum Information Science (QIS)



- Quantifying quantum utility for government and commercial sector
- Mapping applications to algorithms and processors
- Investigating tradeoffs in physical qubit architecture

Quantify and expand the use case for quantum computation

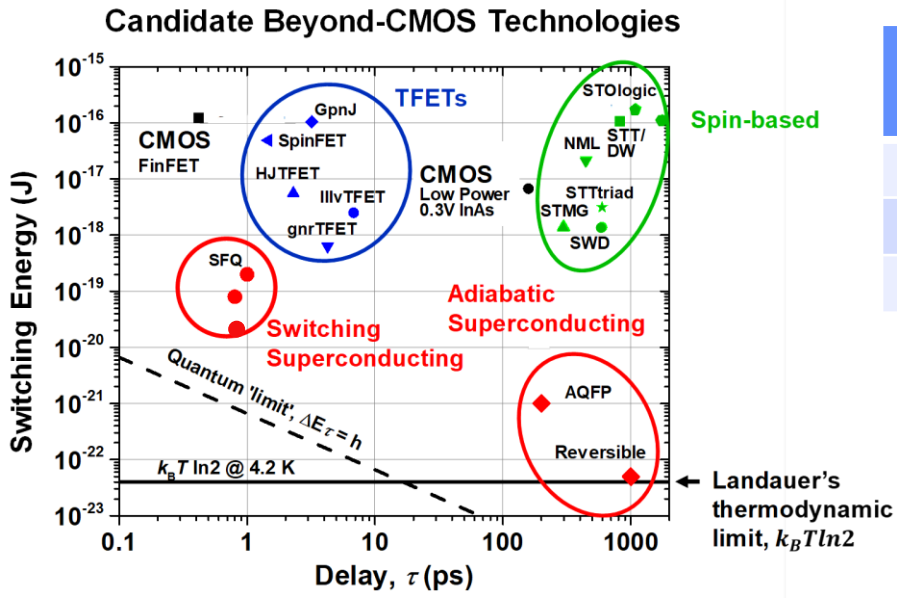


Outline

- ➔ • **Overview of MIT Lincoln Laboratory SCE integrated circuit foundry**
- **SCE digital logic applications and motivation for advanced process nodes**
 - In context of continuing advances in digital CMOS technology
- **Advanced process node development (SFQ7ee)**
 - **Emphasis on increasing SCE circuit density**
 - Compact kinetic inductors
 - Self-shunted Josephson junctions
- **Flux-trapping diagnostics and mitigation**

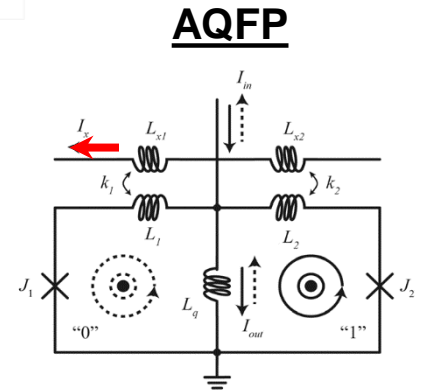
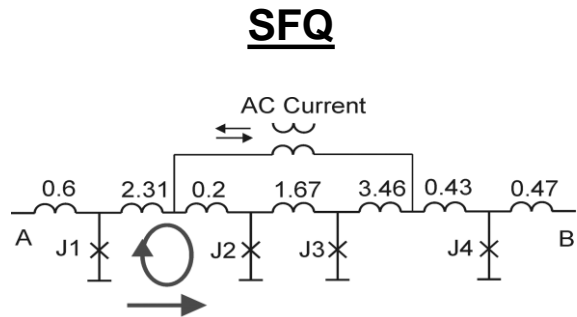


Superconducting Electronics (SCE) for Low-Energy Digital Computation



Logic Element	5-nm CMOS FinFET	SCE AQFP	Energy Ratio CMOS / SCE	
			w/o cooling	w/cooling
4-bit Adder	$8 \cdot 10^{-15}$ J	$8 \cdot 10^{-20}$ J	$\sim 10^5$	$\sim 10^2$
4-bit Multiplier	$4 \cdot 10^{-14}$ J	$4 \cdot 10^{-19}$ J	$\sim 10^5$	$\sim 10^2$
Data Transfer	10^{-13} J/b	10^{-19} J/b	$\sim 10^6$	$\sim 10^3$

- **Lowest energy per digital bit operation**
 - Adiabatic Quantum Flux Parametron (AQFP): $\sim 10^{-21}$ J
- **Highest clock rate in digital circuits**
 - Single Flux Quantum (SFQ): >100 GHz
- **Nearly lossless data transmission: 10^{-19} J/bit**
- **Operates in closed-cycle cryocooler at 4K**

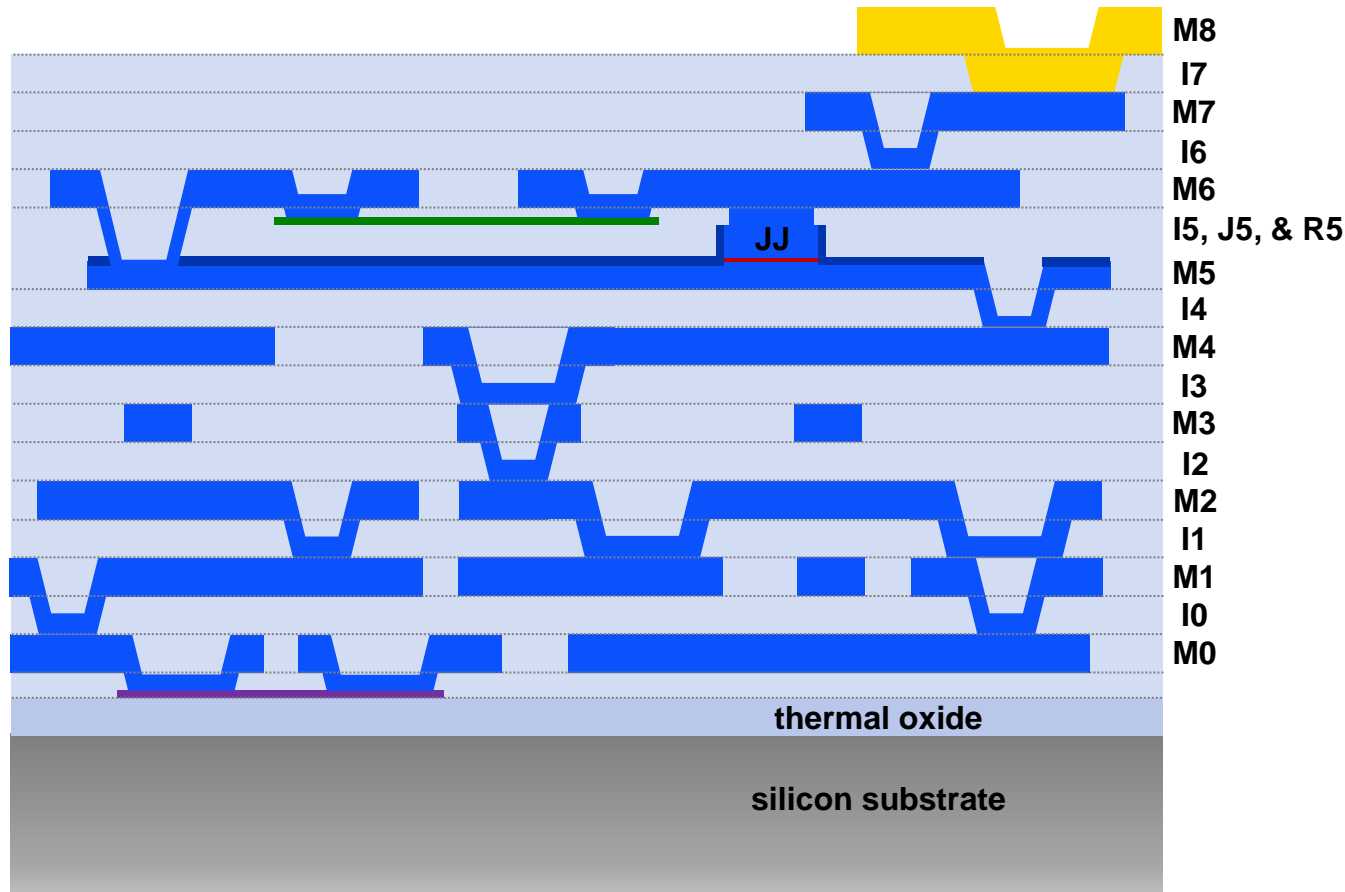


Superconductor electronics (SCE) is the lowest energy of all beyond-CMOS technologies for digital computation



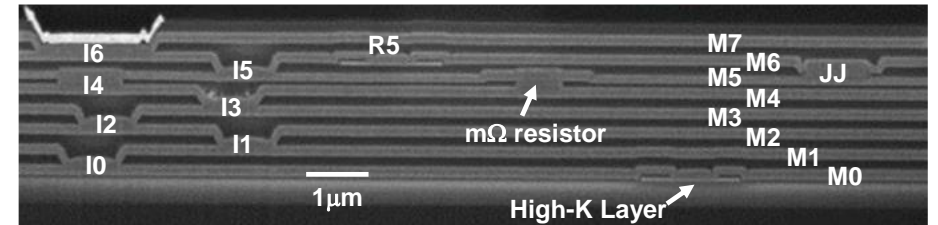
MIT-LL SFQ5ee Research Foundry Process Node

MIT LL SFQ5ee cross section

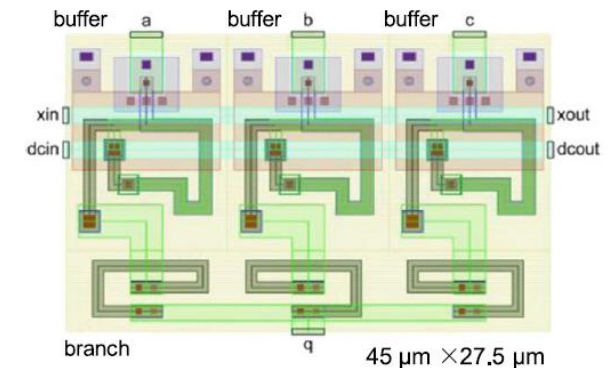


- Nb
- PECVD SiO₂
- JJ barrier
- High kinetic inductor
- Au pad
- Thermal SiO₂
- Anodization
- Shunt resistor

- 8 Nb layers, fully planarized
- 700 nm Josephson junctions (min)
- J_C : standard $100 \mu\text{A}/\mu\text{m}^2$
 - optional 2, 4, 200 & 600 $\mu\text{A}/\mu\text{m}^2$
- Wiring: 250-nm minimum feature size
- Mo₂N high kinetic inductance layer



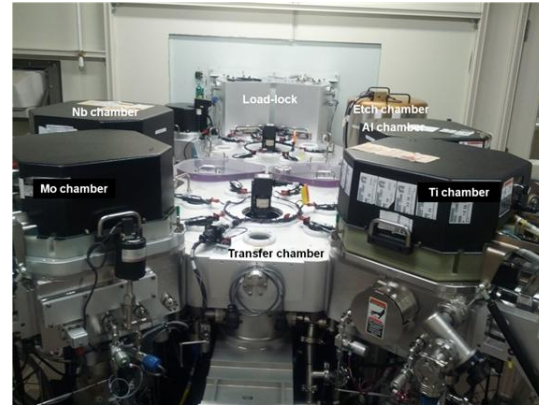
Example SFQ5ee layout: AQFP MAJ3 gate [1]



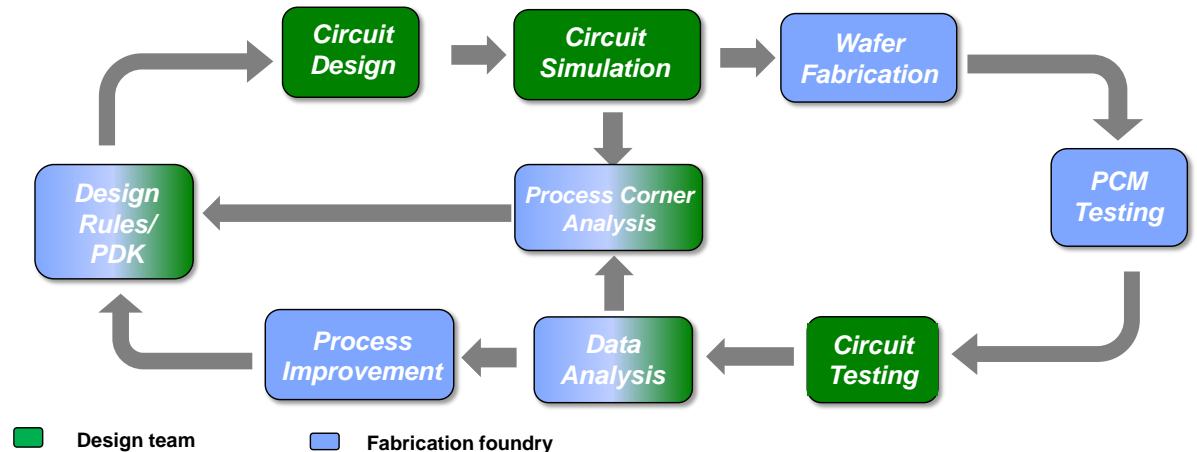
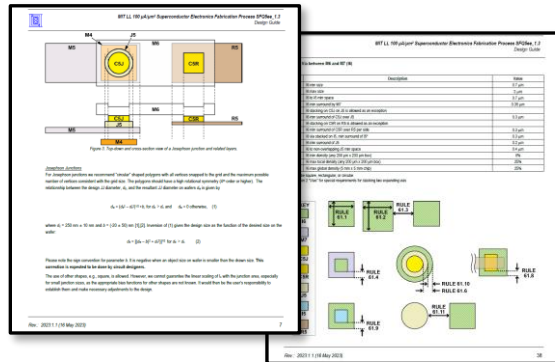


MIT LL Foundry for Superconductor Electronics (SCE)

MIT-LL Microelectronics Laboratory (Class 10, 200-mm wafers)



MIT LL SFQ5ee Design and Modeling Guide

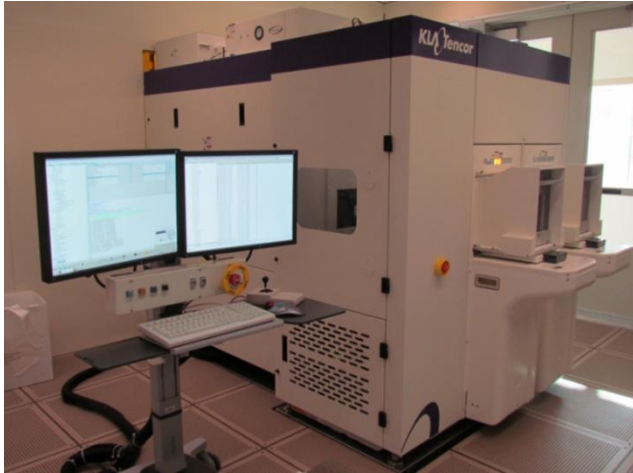


Fabrication capability for advancing the state-of-the-art of SCE integrated circuits



In-Line Defect Inspection

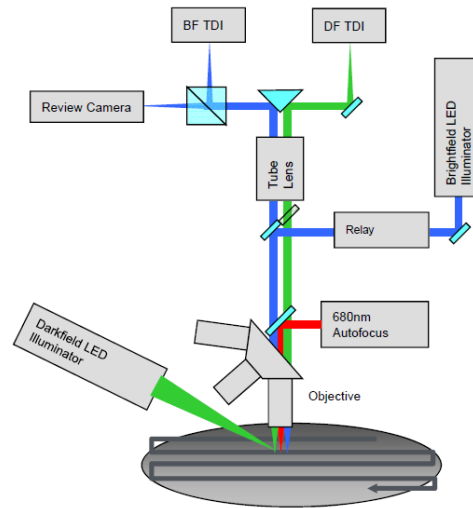
KLA-Tencor Defect Inspection Tool



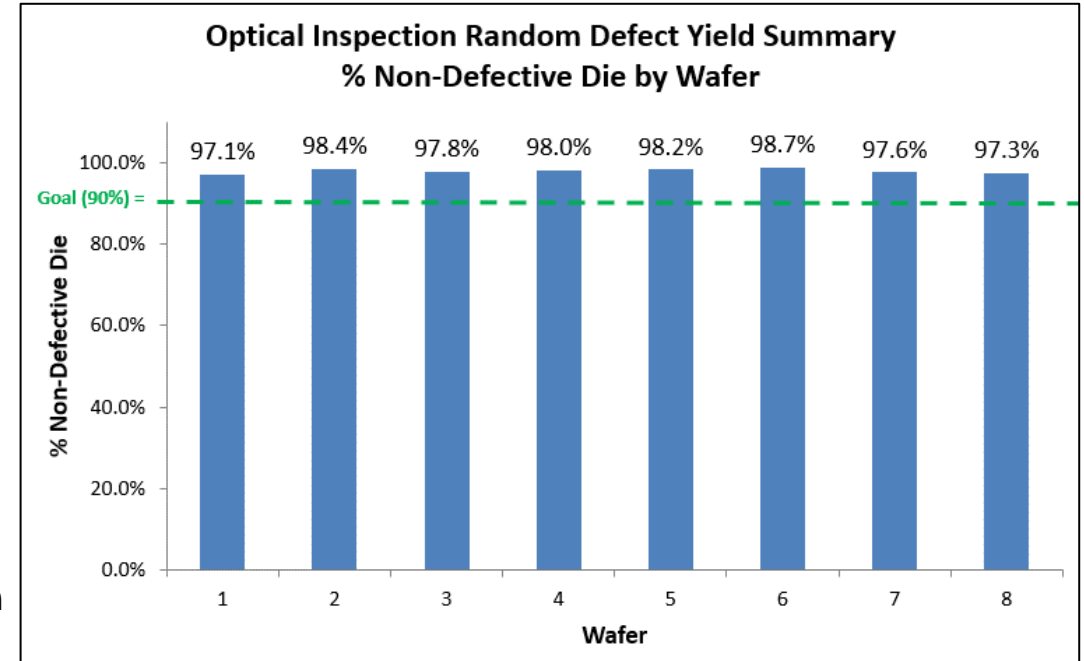
50 wafers/h throughput

- Bright field: Litho and etch defects
- Dark field: Particles & polish defects

~ 100 nm smallest defect detection
(Dark Field)



SFQ5A4 MPW Run (2021)



- SFQ5ee defect-free chip yield typically exceeds 90% for all wafers (as observed on active circuit area)
- Interconnect layer defect density (wafer average per layer) ~ 0.03 defects/cm²
- SFQ5ee wafer average killer defect density ~ 0.3 defects/cm²



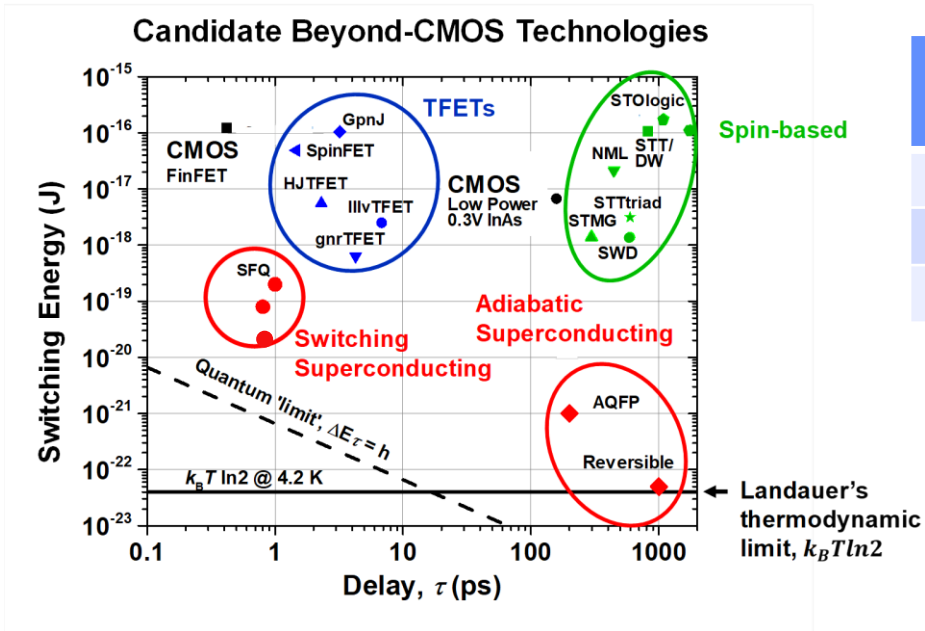
Partners & Sponsors Utilizing MIT-LL SCE Fab Research Foundry



More than 700 publications reference the MIT-LL SFQ5e fabrication process node



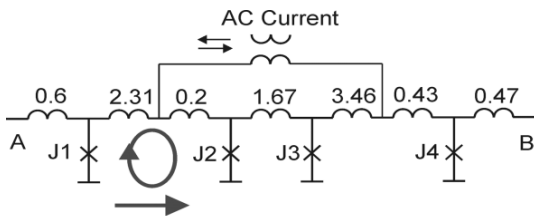
Superconducting Electronics (SCE) for Low-Energy Digital Computation



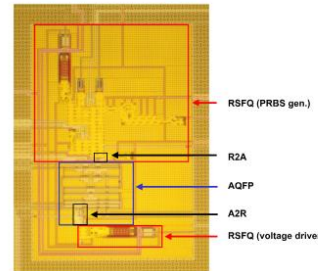
Logic Element	5-nm CMOS FinFET	SCE AQFP	Energy Ratio CMOS / SCE	
			w/o cooling	w/cooling
4-bit Adder	$8 \cdot 10^{-15}$ J	$8 \cdot 10^{-20}$ J	$\sim 10^5$	$\sim 10^2$
4-bit Multiplier	$4 \cdot 10^{-14}$ J	$4 \cdot 10^{-19}$ J	$\sim 10^5$	$\sim 10^2$
Data Transfer	10^{-13} J/b	10^{-19} J/b	$\sim 10^6$	$\sim 10^3$

- **Lowest energy per digital bit operation**
 - Adiabatic Quantum Flux Parametron (AQFP): $\sim 10^{-21}$ J
- **Highest clock rate in digital circuits**
 - Single Flux Quantum (SFQ): >100 GHz
- **Nearly lossless data transmission: 10^{-19} J/bit**
- **Operates in closed-cycle cryocooler at 4K**

Example Schematic

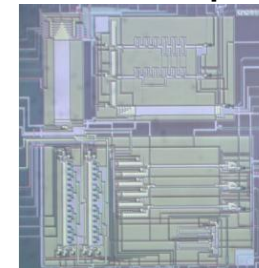


SFQ5ee AQFP/SFQ interface



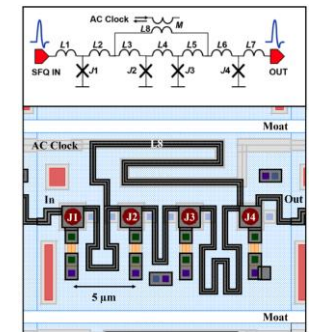
YNU & Hypres, Inc

SFQ data transmission test chip



Hypres, Inc

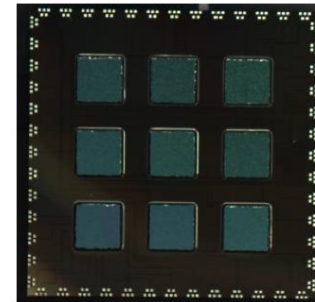
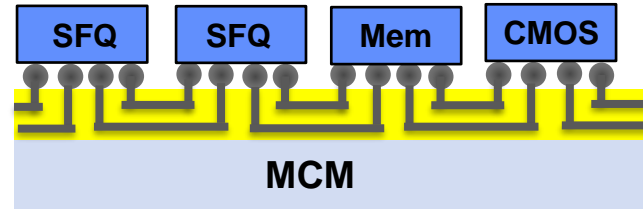
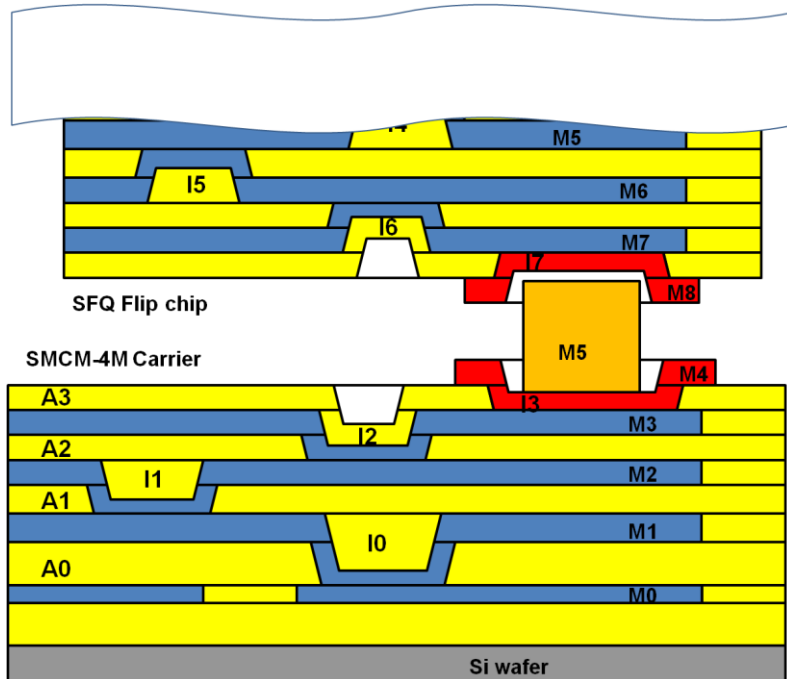
MIT-LL Shift Register
~1M JJs



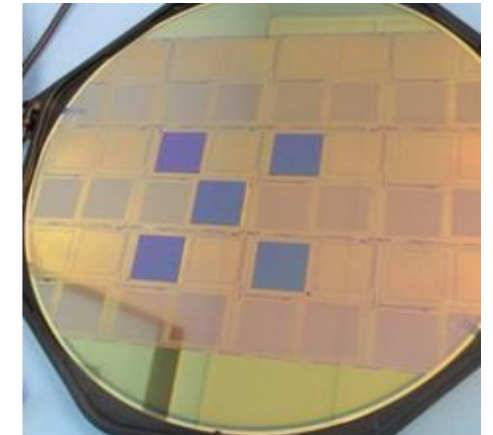
Superconductor electronics (SCE) is the lowest energy of all beyond-CMOS technologies for digital computation



Flip-Chip Superconducting MCM Packaging



9-chip (Northrop Grumman RQL)
on S-MCM assembly
IARPA C3 Program



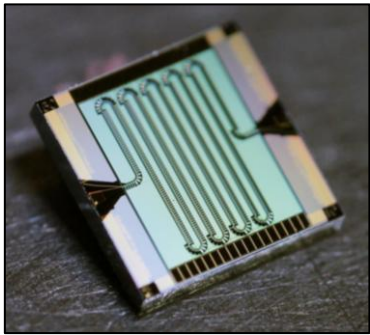
Wafer-scale S-MCM with 800-nm
minimum linewidth (utilizing
stitching)

- Flip-chip attachment of SFQ (and other) chips to S-MCM carriers
- Provides controlled-impedance transmission lines between chips
- Indium bumps: down to 5 μm pitch
- 32 mm x 32 mm MCM size (up to 5 cm by 5 cm possible)

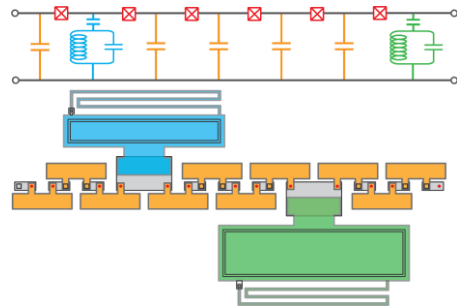


Traveling-Wave Parametric Amplifiers (TWPAs) for Superconducting Qubit Diagnostics

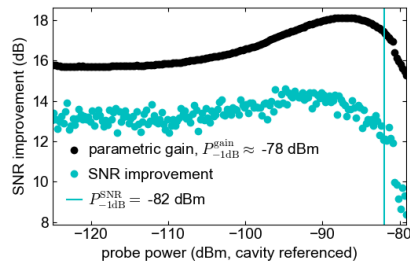
Research and Development for TWPAs



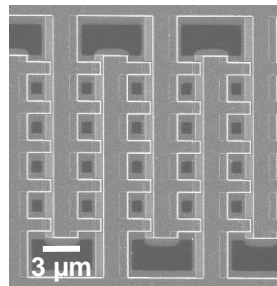
“OG” MIT LL JTWSA [1]



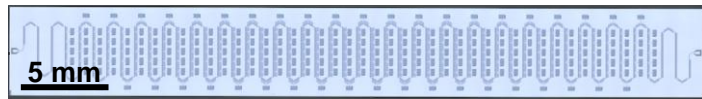
Dual-pumped JTWSA for broadband two-mode squeezing [2]



High-Dynamic Range JTWSAs

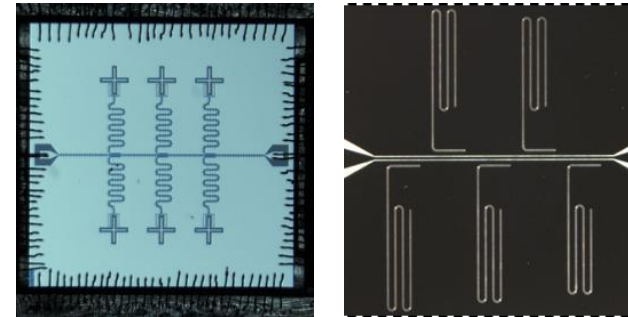


Low-Loss Parallel-Plate Capacitors

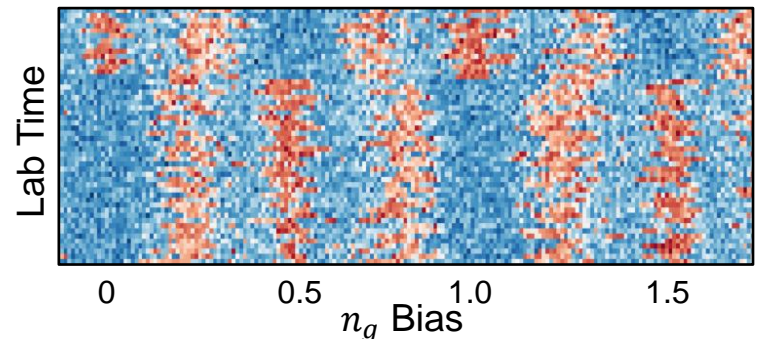


Floquet-Mode JTWSA [3]

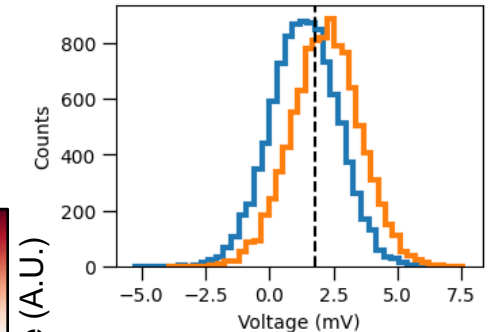
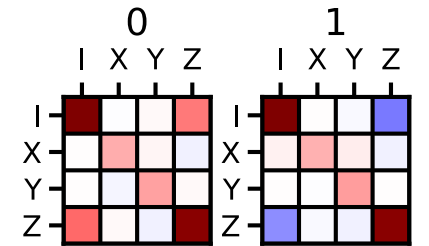
TWPAs for Research and Development



Candle qubits/witness resonators: >1,000 characterized per year



Single-shot measurement-based discrimination between charge offset drift and parity jumps



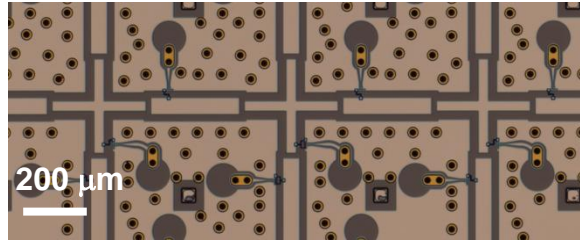
QCVV protocols for mid-circuit measurements



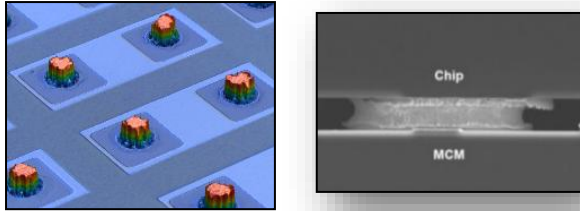
Heterogeneous Multi-Tier Qubit Integration Platform

Incorporates Nb Routing based on SFQ5ee node

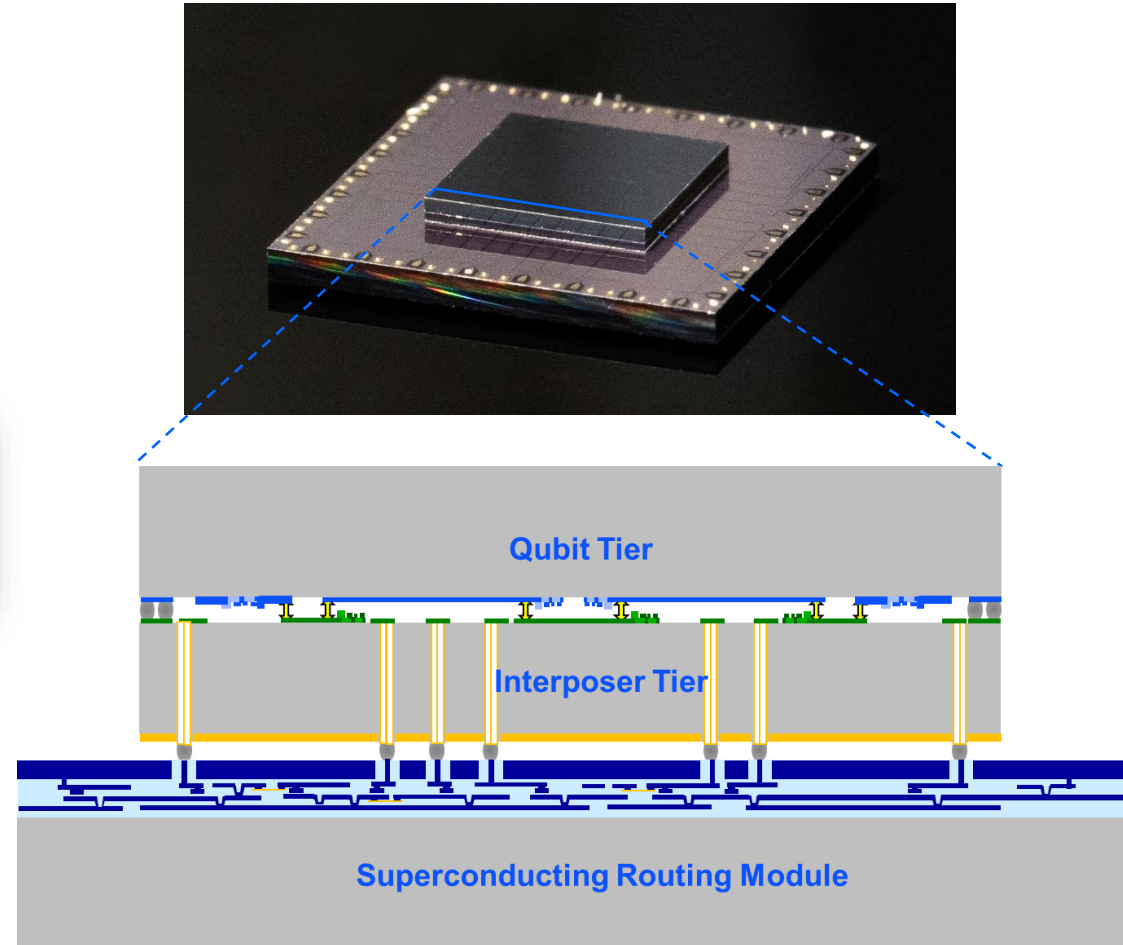
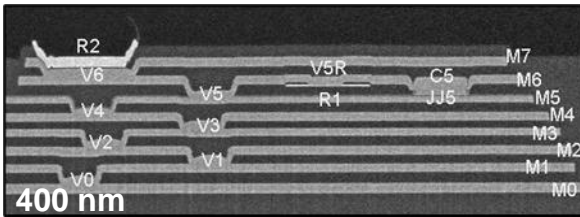
Superconducting Qubits



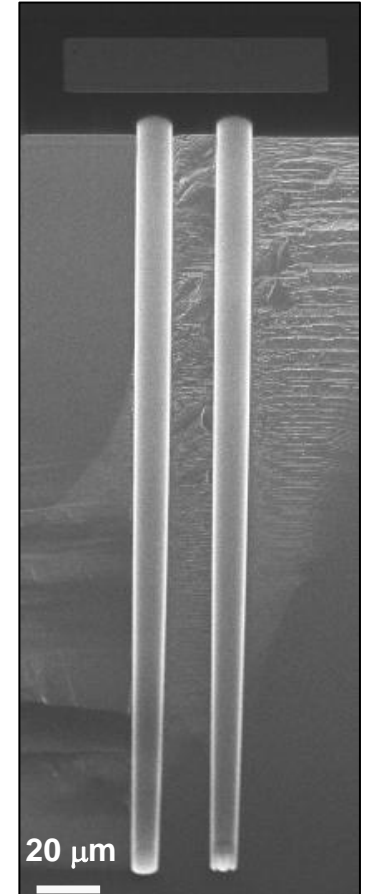
Indium Bump Interconnects



Multilayer Niobium Routing



Through-Silicon Vias



Multi-tier stacks aim to enable high connectivity while maintaining qubit coherence



Superconducting mm-Wave Filters in SFQ5ee U Waterloo

Millimeter-Wave Ultra Wideband Multilayer Superconducting Filter

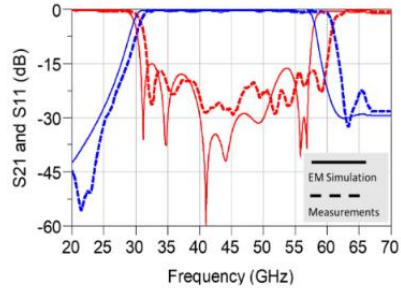


Fig. 12. Simulation and measurement results.

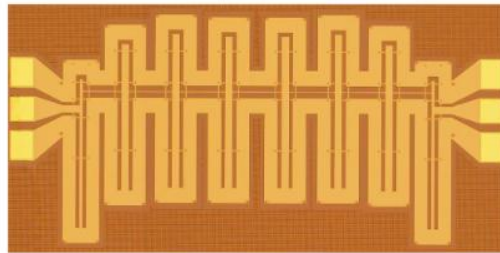


Fig. 2. Photo of the fabricated multilayer superconductor filter.

**Coplanar Waveguide (CPW) 8-pole design (0.9 x 2.2 mm²)
Fabricated at MIT-LL in the SFQ5ee process (no JJ's)**

Mansour, *IEEE Microwave Magazine* (June 2025)

Jia and Mansour, *IEEE Trans. Appl. Superconductivity* 29 (2019)

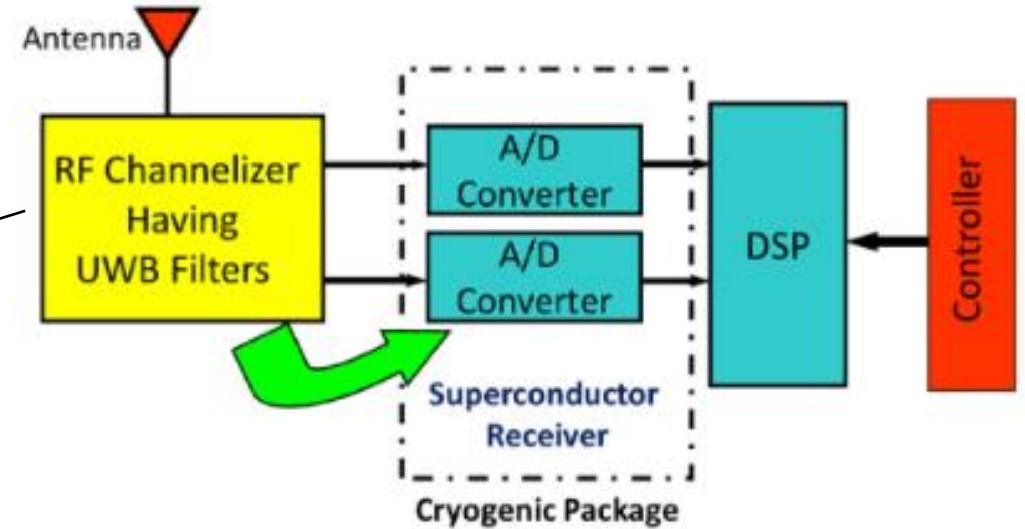


Fig. 1. Schematic block diagram of superconductor digital receiver.



UNIVERSITY OF
WATERLOO



SCE fabrication processes (SFQ5ee) enable integration of passive microwave/mm-wave elements with active circuits

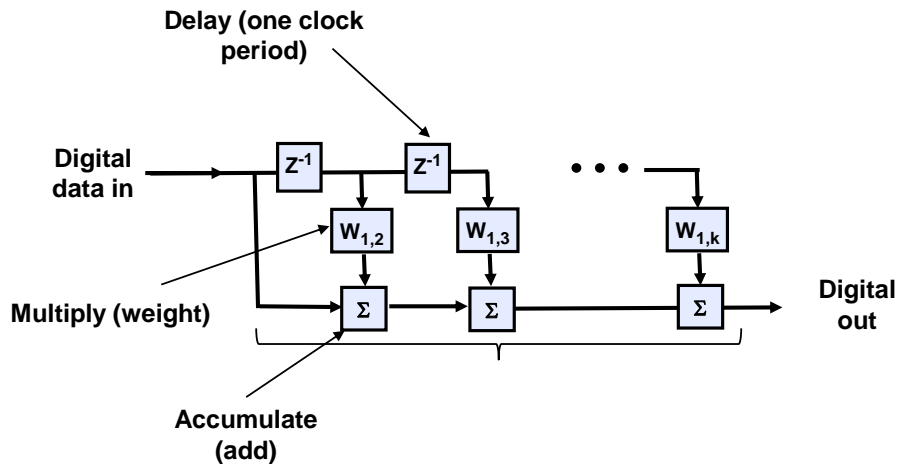
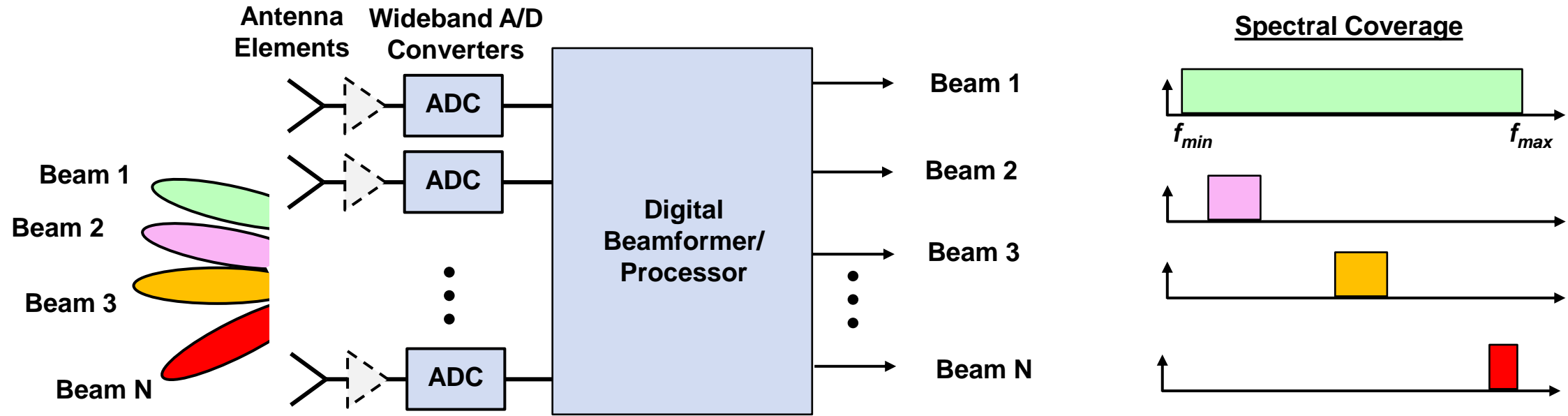


Outline

- Overview of MIT Lincoln Laboratory SCE integrated circuit foundry
- ➔ • SCE digital logic applications and motivation for advanced process nodes
 - In context of continuing advances in digital CMOS technology
- Advanced process node development (SFQ7ee)
 - Emphasis on increasing SCE circuit density
 - Compact kinetic inductors
 - Self-shunted Josephson junctions
- Flux-trapping diagnostics and mitigation



Multi-Beam Multi-Function Digital Array Sensor/Receiver for Wideband RF/mm-wave Systems



- Digital arrays offer highly agile independent beams
- Digital processing dominated by multiply/accumulate operations (FIR filtering)
 - Often with modest memory requirements
- Increasing energy efficiency of digital process enables wideband & high-beam-count systems
- Need for low-power (including cooling) digital processors with >10's petaFLOPS performance



Ongoing Advances in Si CMOS Digital Logic

SPECIAL SECTION TRANSISTORS

Datta et al., Science 378, 733-740 (2022) 18 November 2022

REVIEW

Toward attojoule switching energy in logic transistors

Suman Datta^{1,2*}, Wriddhi Chakraborty², Marko Radosavljevic³

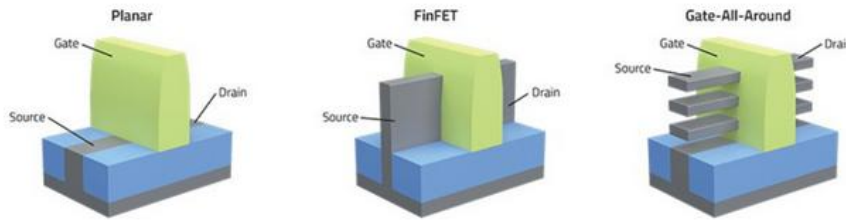
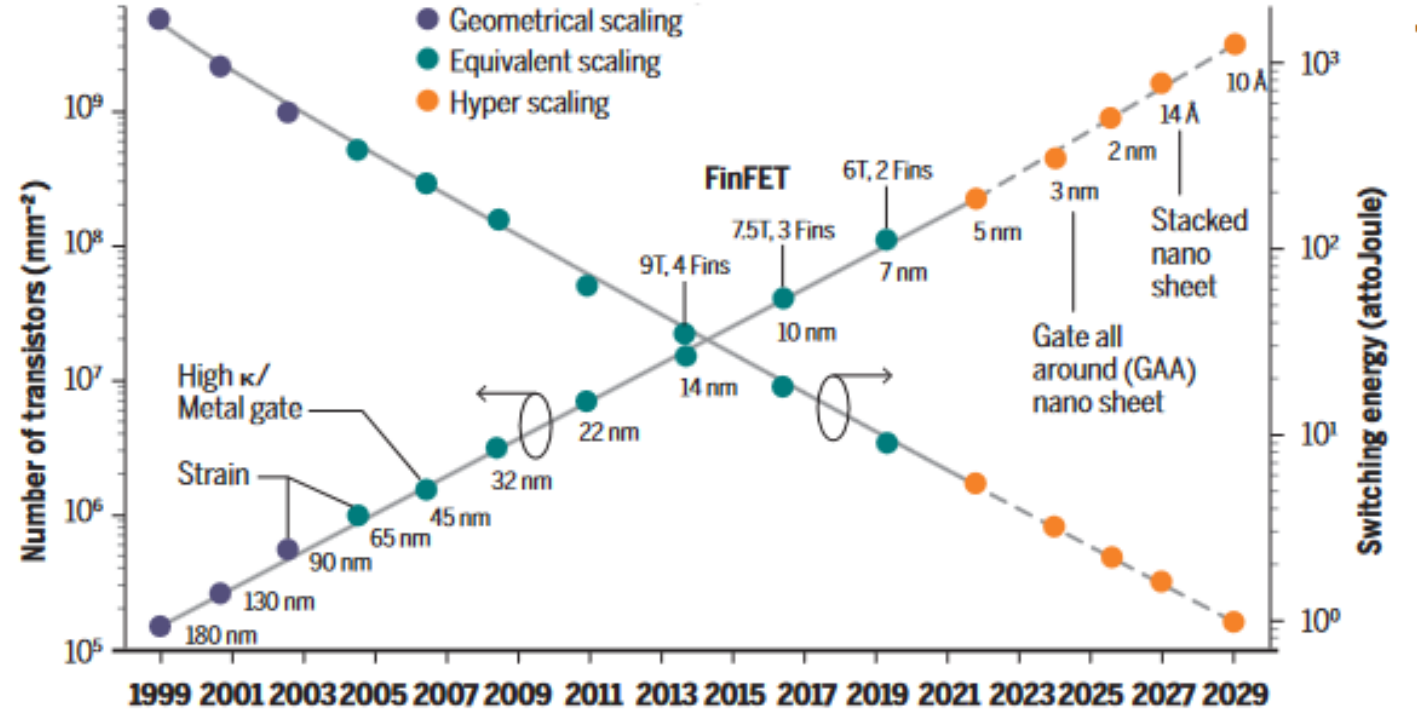


Fig. 1: Planar transistors vs. finFETs vs. gate-all-around Source: Lam Research

TSMC's 2nm N2 process node enters production this year, A16 and N2P arriving next year

News By Anton Shilov published April 24, 2025

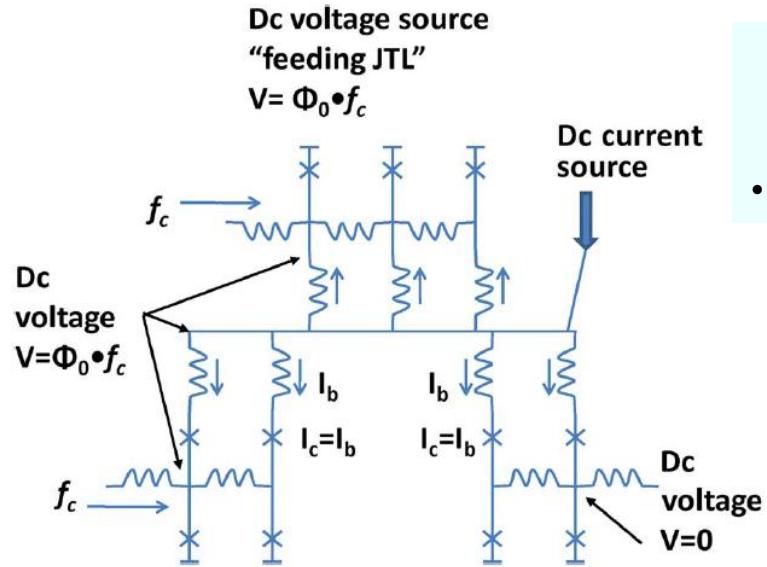
tom's HARDWARE



While logic transistor switching energy continues to decline, energy per OP in logic circuits and processors will likely be dominated by other factors (interconnects, etc.)



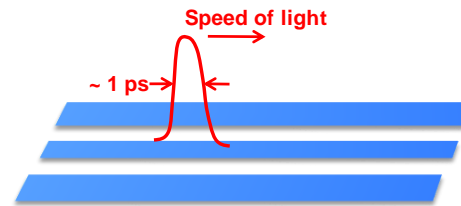
SFQ Logic Families



Energy-Efficient RSFQ (ERSFQ)

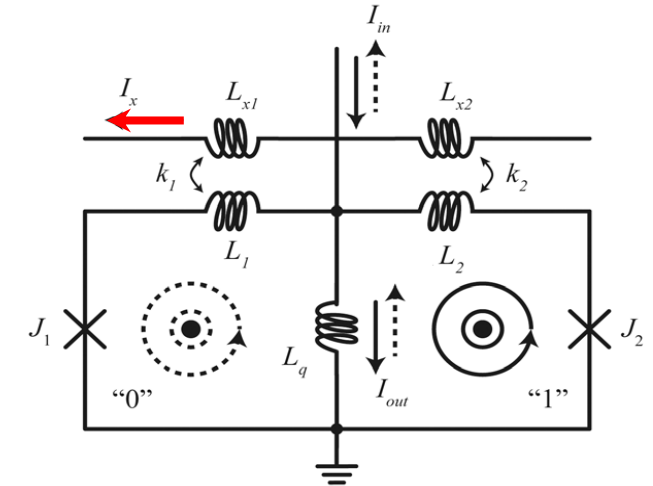
- Eliminates resistor-based bias network

Lossless SFQ data transmission



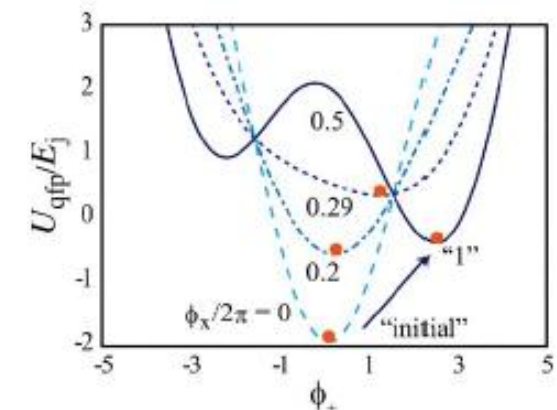
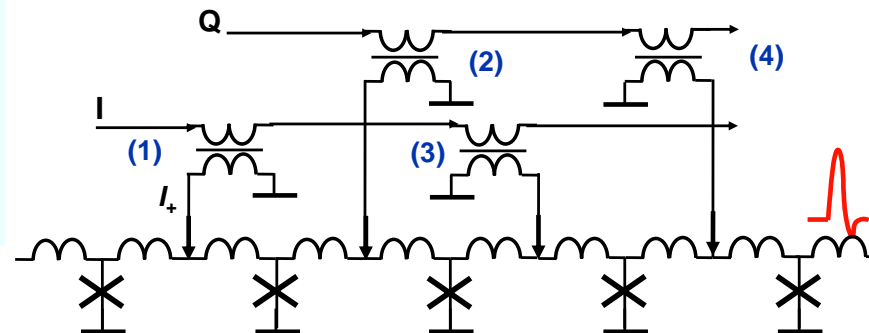
Adiabatic Quantum Flux Parametron (AQFP)

- JJs do not 'switch'



Reciprocal Quantum Logic (RQL)

- Developed by Northrop Grumman
- Based on AC biasing





AQFP Energy Dissipation

PHYSICAL REVIEW APPLIED 4, 034007 (2015)

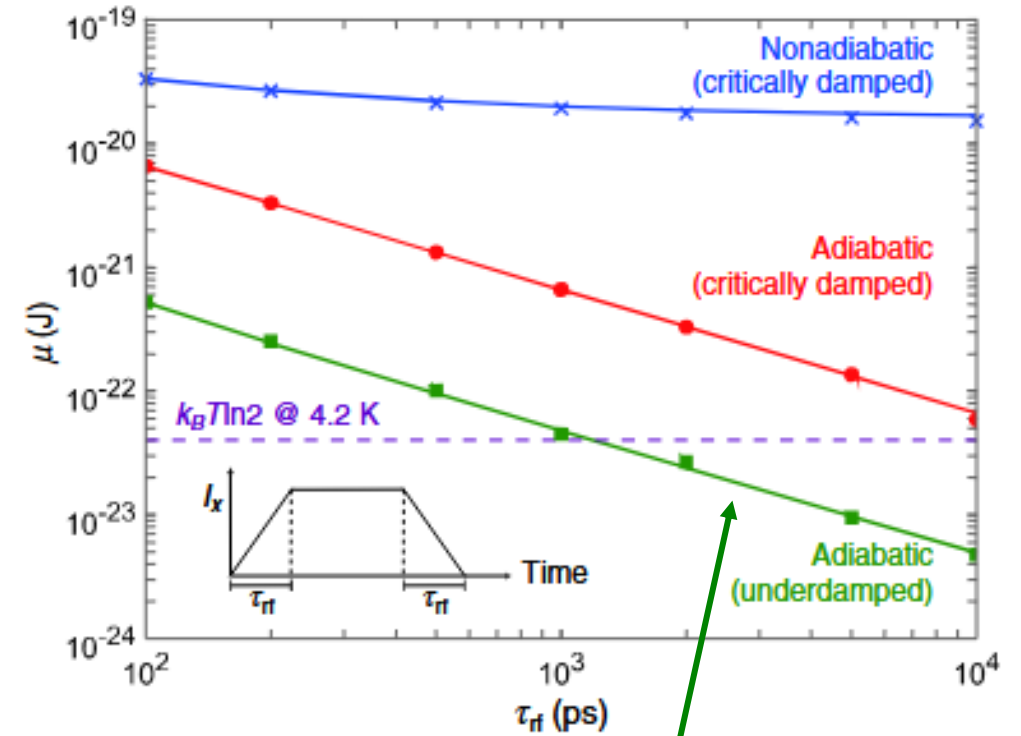
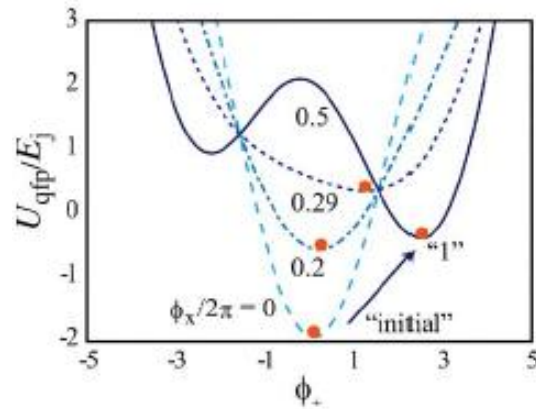
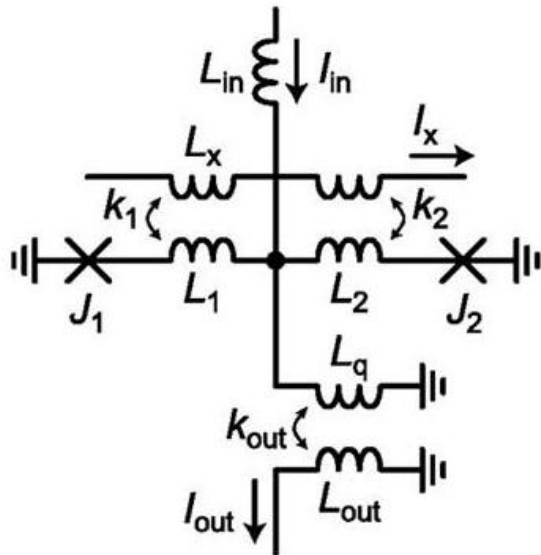
Thermodynamic Study of Energy Dissipation in Adiabatic Superconductor Logic

Naoki Takeuchi,^{1,*} Yuki Yamanashi,^{1,2} and Nobuyuki Yoshikawa^{1,2}

¹Institute of Advanced Sciences, Yokohama National University,
79-5 Tokiwadai, Hodogaya, Yokohama 240-8501, Japan

²Department of Electrical and Computer Engineering, Yokohama National University,
79-5 Tokiwadai, Hodogaya, Yokohama 240-8501, Japan

(Received 17 June 2015; revised manuscript received 28 June 2015; published 24 September 2015)



$$\beta_L = \frac{2\pi I_{CJ} L_2}{\Phi_0} = 0.2$$

$$\beta_q = \frac{2\pi I_{CJ} L_q}{\Phi_0} = 1.6$$

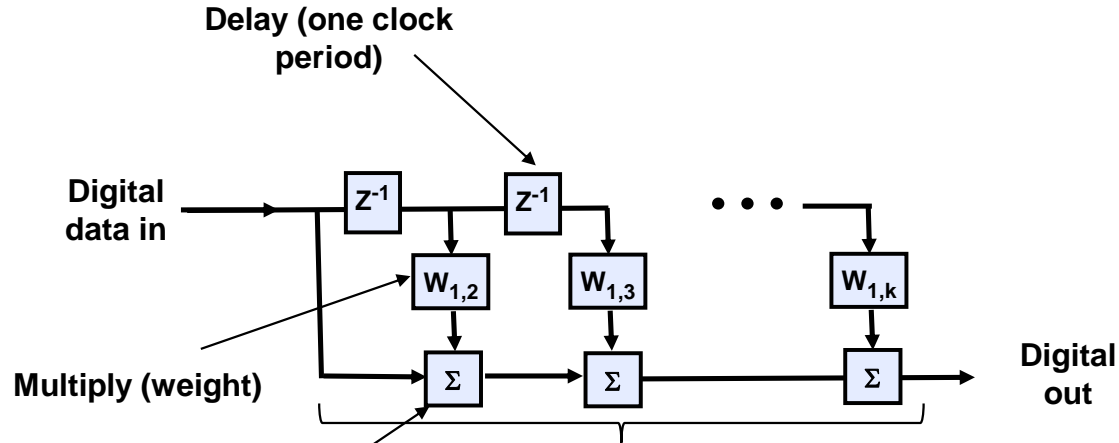
$$I_{CJ} = 50 \mu\text{A}$$

No external shunt resistor

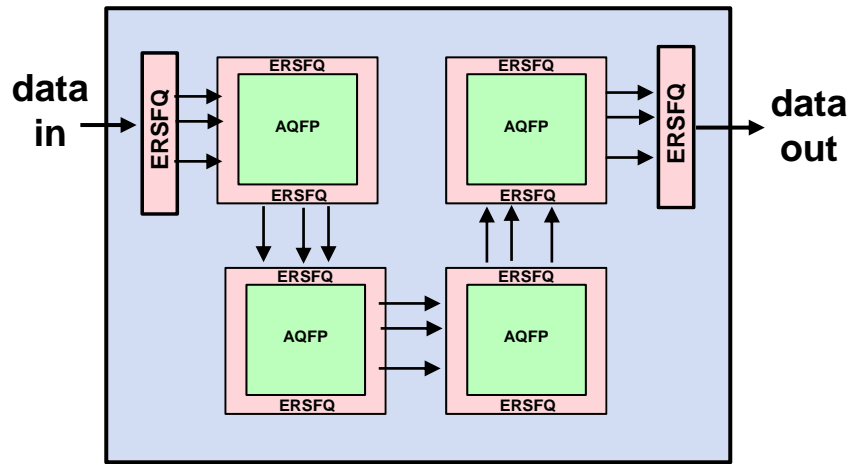


Dataflow FIR Filter

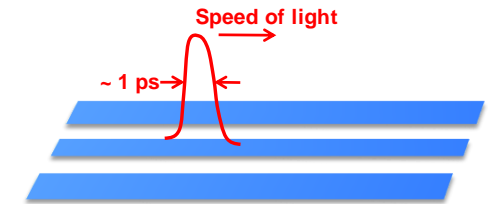
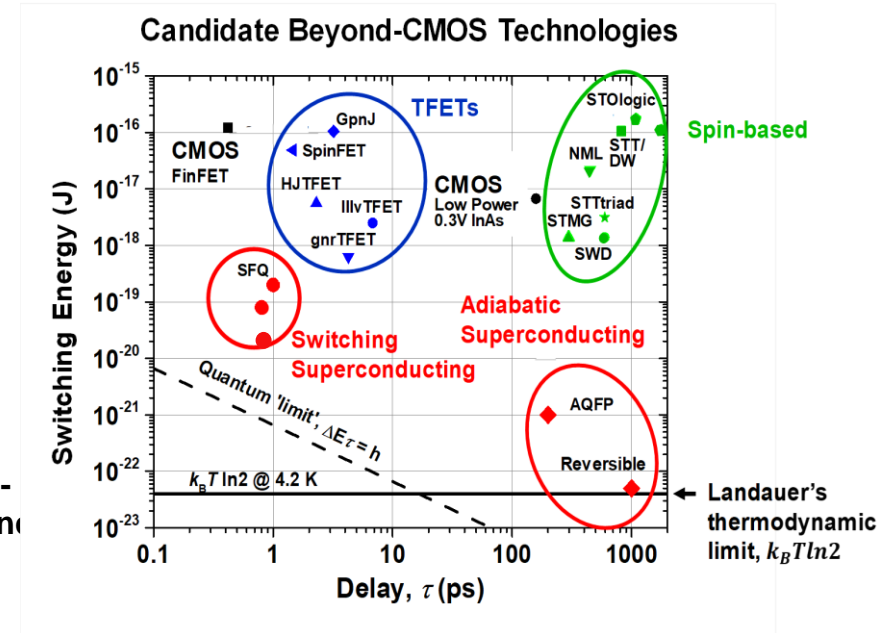
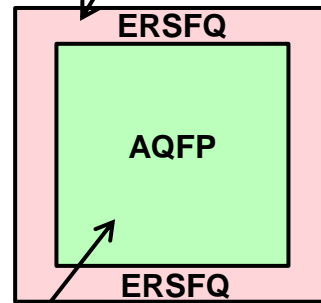
Hybrid ERSFQ/AQFP Superconducting Electronics



ERSFQ circuitry (as needed) for high-speed low-energy data transmission and interfaces



AQFP circuitry for low-energy digital computation



SFQ pulse ballistic data transport on superconducting transmission line

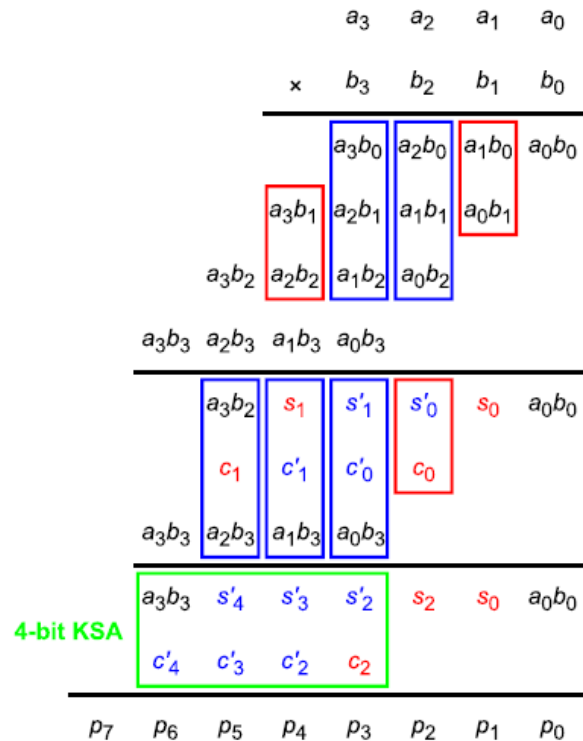


Demonstrated AQFP Multiplier (2025)

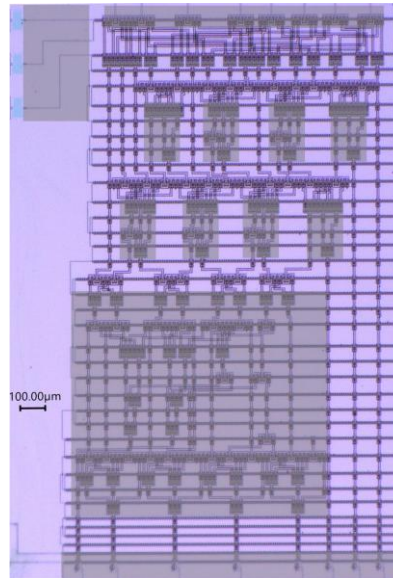
Yokohama National University (YNU)

- Design & demonstration of Array and Wallace-Tree multipliers
 - AIST 10 kA/cm² high-speed standard fabrication process

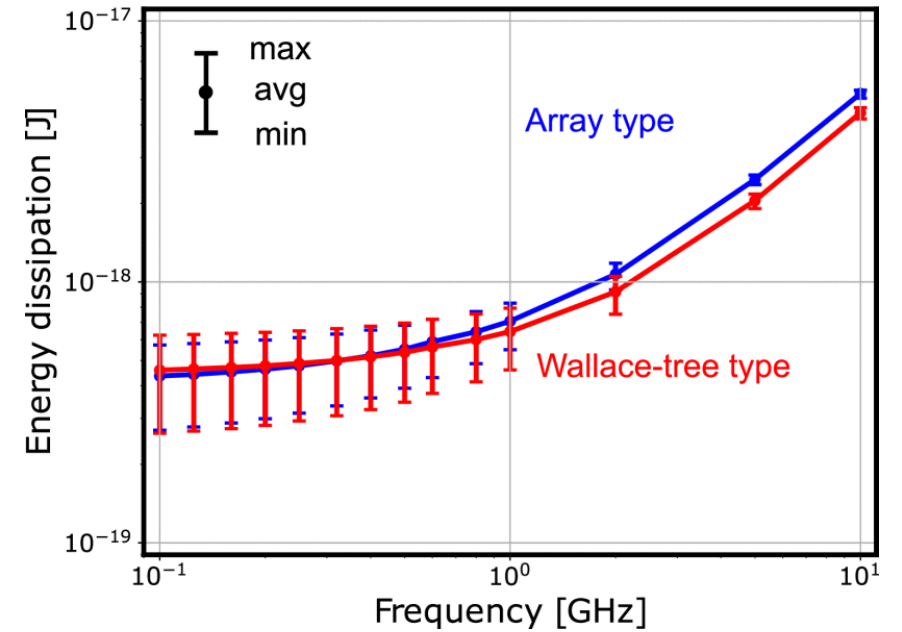
Wallace-tree multiplication



Wallace-tree multiplier chip



1624 JJs
1.6 x 2.5 mm

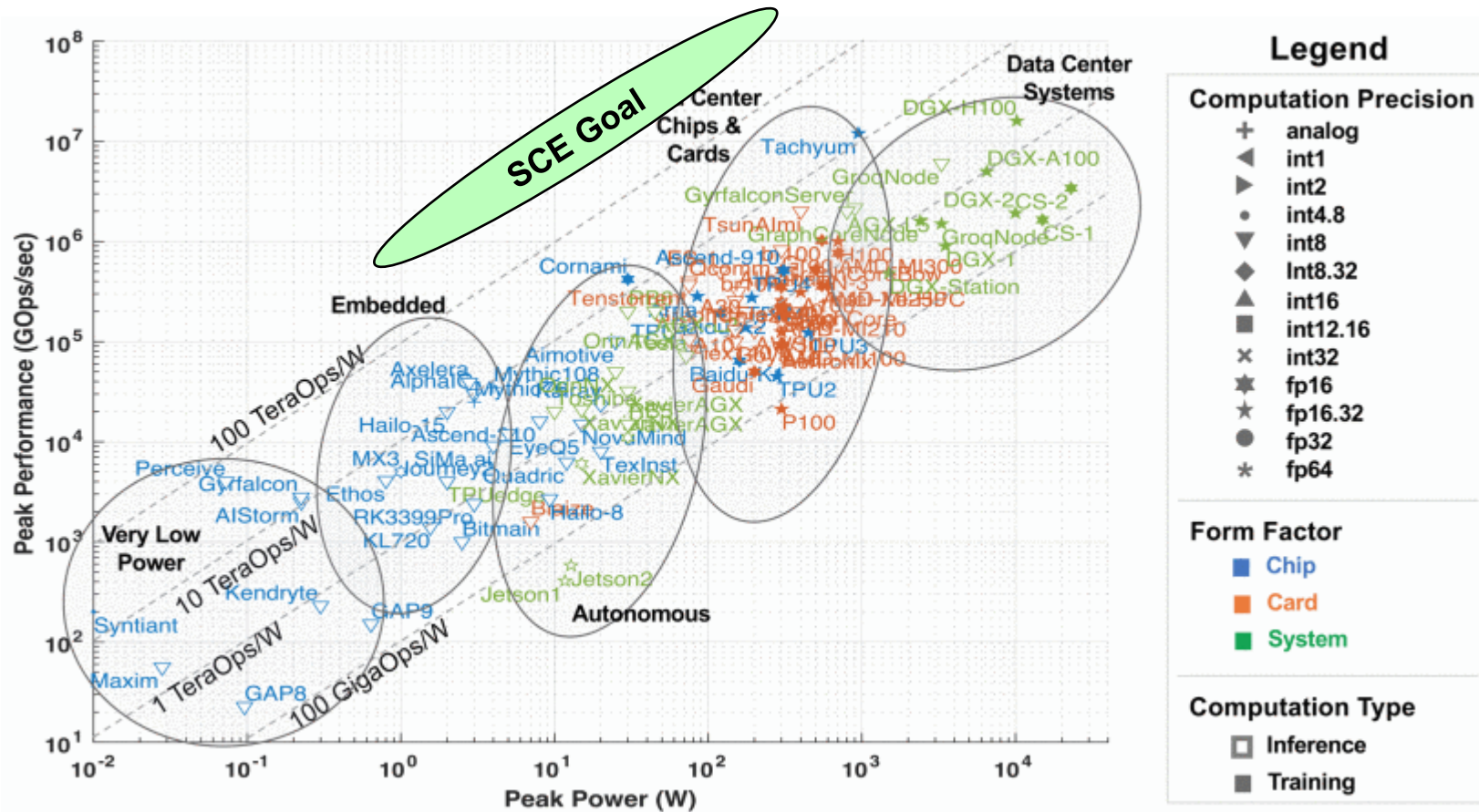


Multiplier energy
~6x10⁻¹⁹ J @ 1 GHz



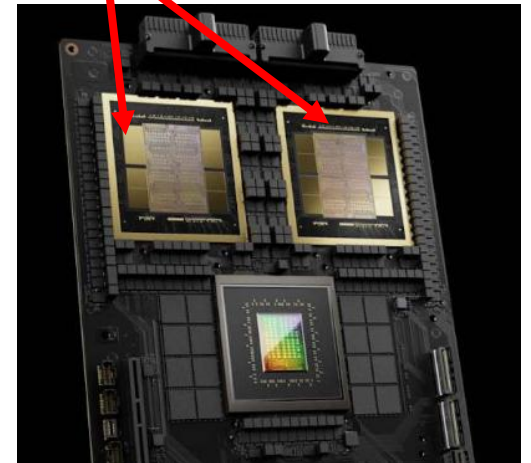
Lincoln AI Computing Survey (LAICS)

Reuther et al, MIT Lincoln Laboratory
Presented at 2023 IEEE High Performance Extreme
Computing Conference (HPEC)



NVIDIA GB200 Superchip (2024)

Two Blackwell GPUs
208B Transistors



20 petaFLOPS @ 2700 W
 ~ 10⁻¹³ J/FLOP
 → 10 TOPS/W



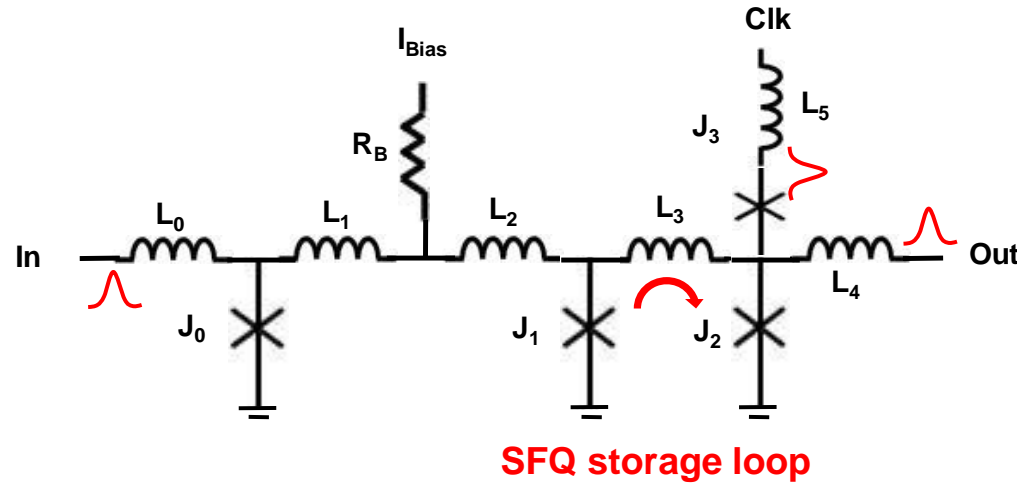
Outline

- **Overview of MIT Lincoln Laboratory SCE integrated circuit foundry**
- **SCE digital logic applications and motivation for advanced process nodes**
 - In context of continuing advances in digital CMOS technology
- ➔ • **Advanced process node development (SFQ7ee)**
 - **Emphasis on increasing SCE circuit density**
 - Compact kinetic inductors
 - Self-shunted Josephson junctions
- **Flux-trapping diagnostics and mitigation**



SFQ D flip-flop (DFF)

Example layout for 4-layer process (circa 2013)



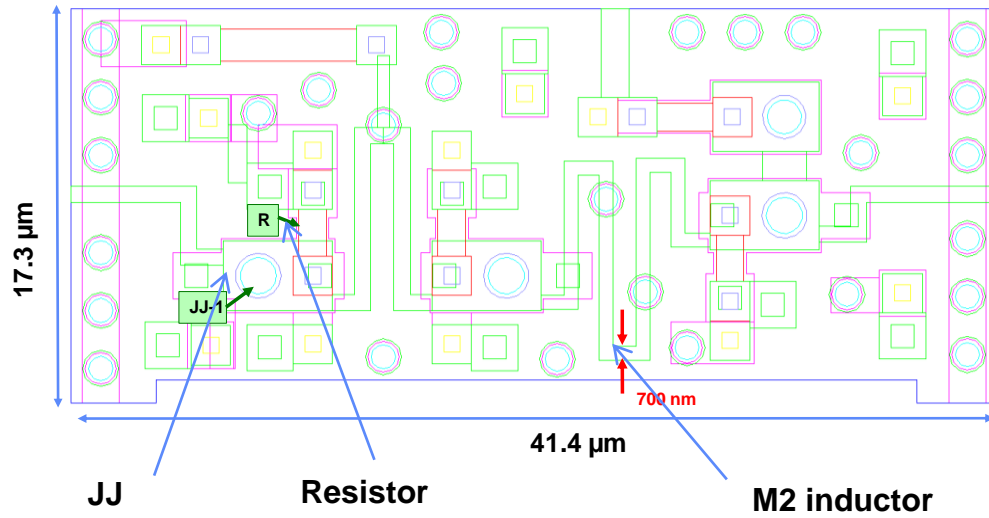
$$\text{Flux quantum } \Phi_0 = h/2e \approx 2 \text{ mV ps}$$

$$E \approx I_C \Phi_0 \sim 10^{-19} \text{ J}$$

- Reducing I_C lowers switching energy, but min I_C limited by thermal error rate
- Min I_C typically 10's μA

$$LI_C \sim \Phi_0$$

- Lower I_C calls for larger L's
- Implications for circuit density
- Geometric inductance per unit length varies inversely with linewidth

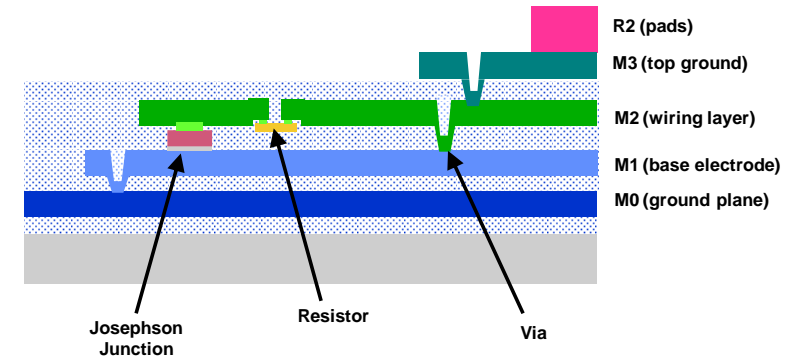


I_C 's $\sim 100 \mu\text{A}$

L's $\sim 5 \text{ pH}$

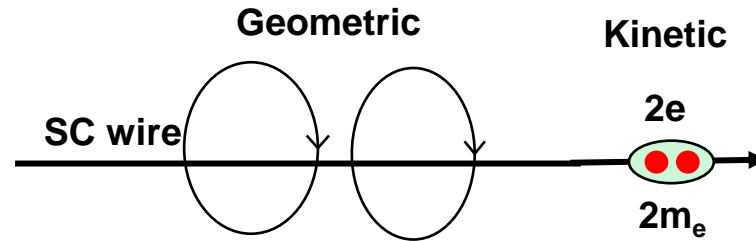
Legacy fab process

For min 700 nm linewidth:
 $L \sim 0.2 \text{ pH}/\mu\text{m}$ (geometric)
 $\sim 1\text{M JJs}/\text{cm}^2$

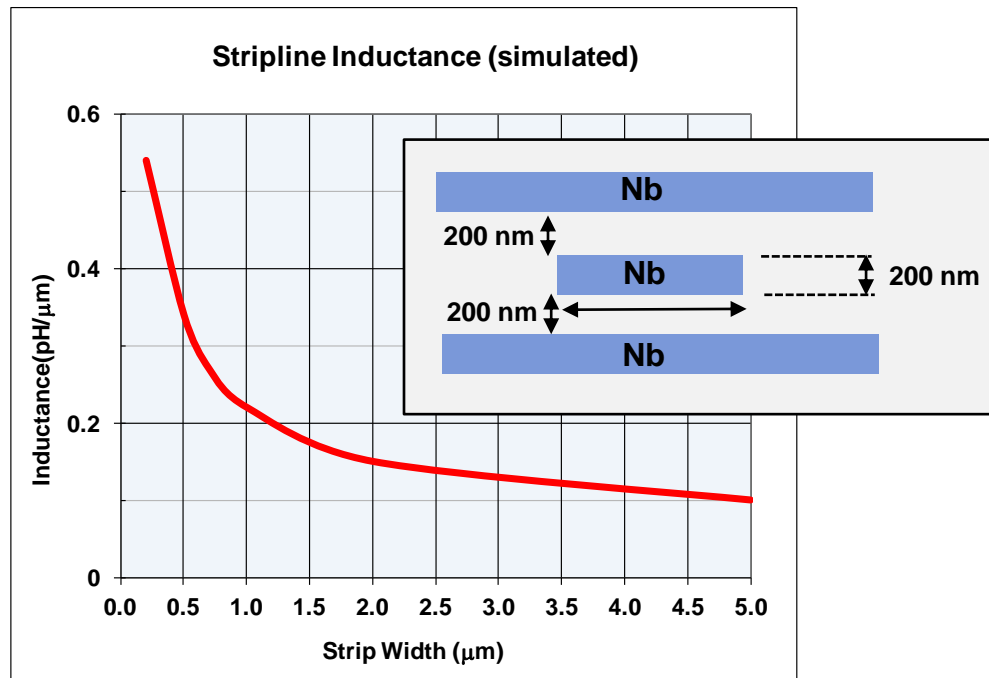




Inductance in Superconducting Wires

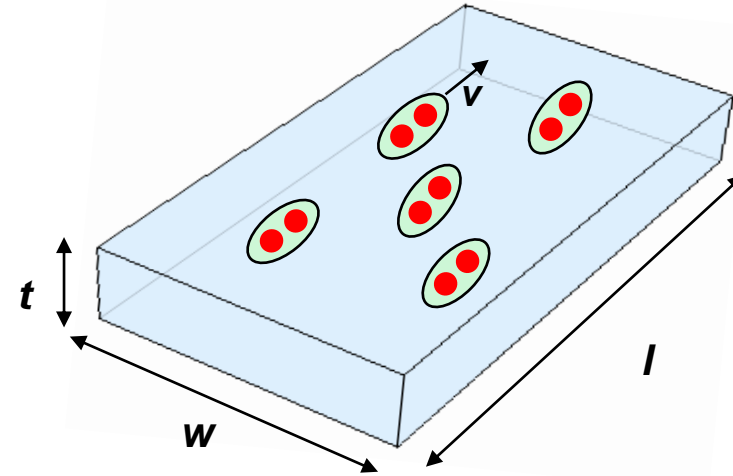


Geometric Inductance



Geometric inductance increases with decreasing linewidth.

Kinetic Inductance



- Superconducting current: $2e$, $2m_e$, velocity v , Cooper pair density n_s ; Penetration depth: λ

$$\frac{L_K}{l} = \left(\frac{m_e}{2n_s e^2} \right) \left(\frac{1}{tW} \right) = \frac{\mu_0 \lambda^2}{tW} \sim 4 \text{ pH}/\mu\text{m for NbN}$$

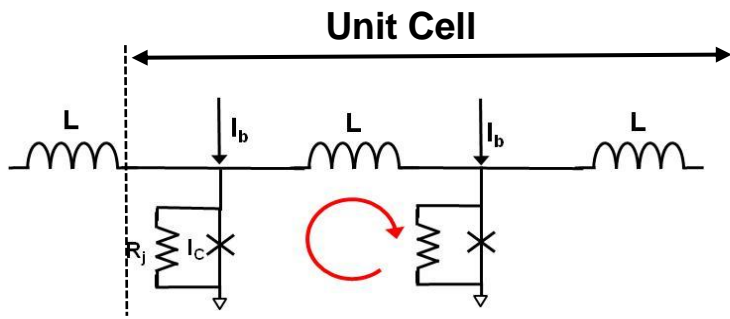
Kinetic inductance varies quadratically with λ , and inversely with cross-section area.



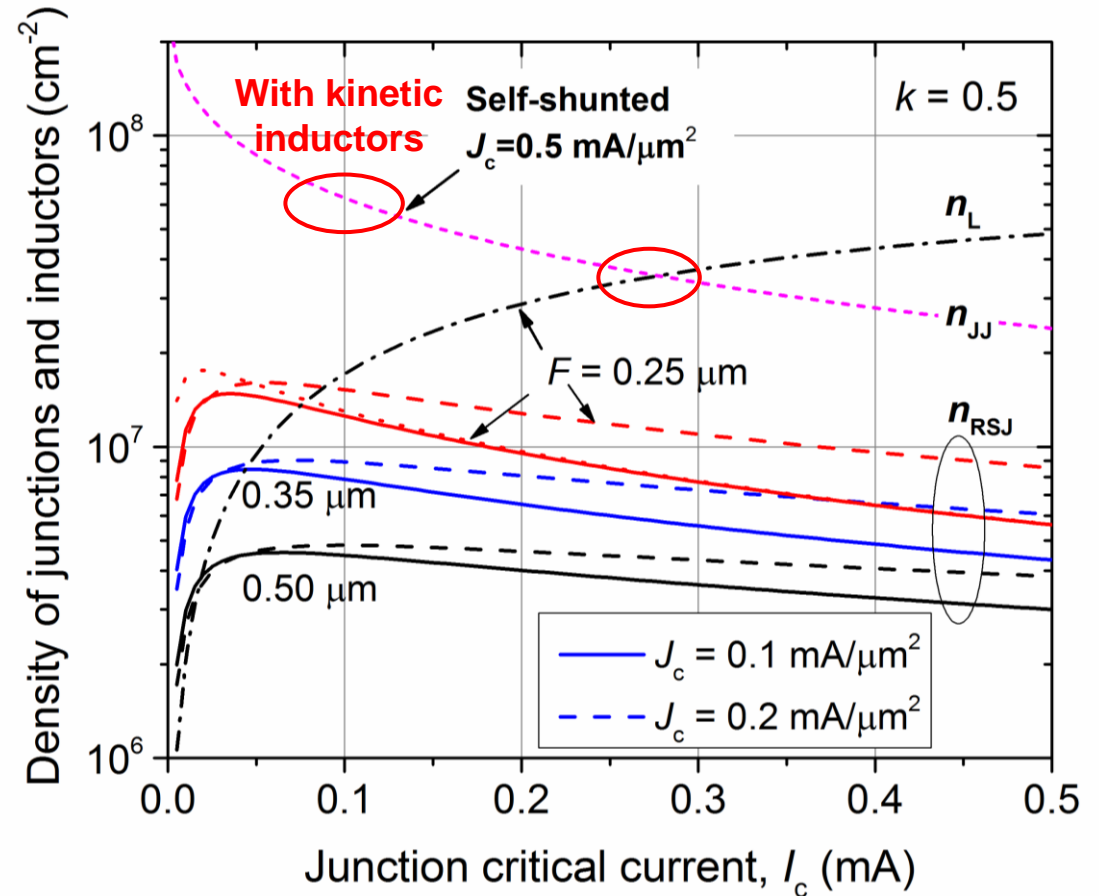
SFQ Circuit Density Drivers: Junctions and Inductors

Pathway Towards $\sim 10^8$ JJs/cm²

- SCE scaling needs to include both Josephson junctions (JJs) and inductors
 - About 1:1 ratio required
 - $LI_c \sim \text{Const.}$
- Maximum circuit density when inductor density matches JJ density, $n_L \sim n_{JJ}$
- Reducing minimum feature size F results in more compact geometric inductors
 - Suitable for externally shunted JJs
- Replace geometric inductors with kinetic inductors with $L_{sq} \sim 4\text{pH/sq}$ further increases density
 - Combine with self-shunted JJs



Component Requirements for Higher Density SCE Circuits





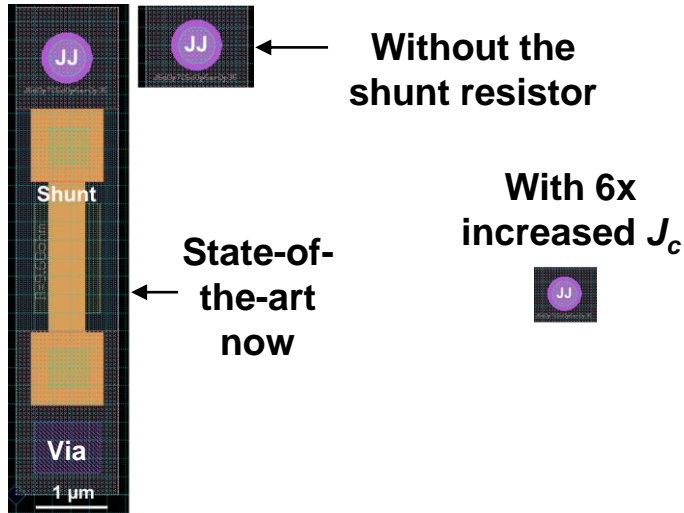
SFQ7ee Process Development Goals

- Develop advanced materials and fabrication technology for a 10x increase in the integration scale of superconductor integrated circuits

Three Major Development Areas

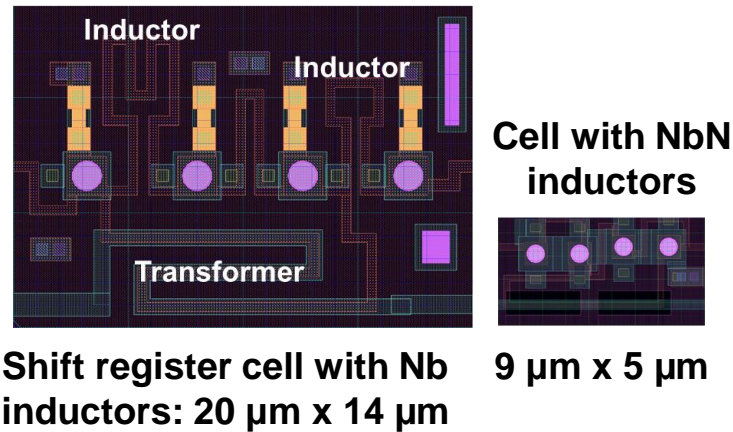
Reduce Area of Active Devices - Josephson Junctions (JJs)

- Develop self-shunted JJs with high critical current density (high- J_c) to
 - eliminate resistive shunts
 - reduce the JJ area



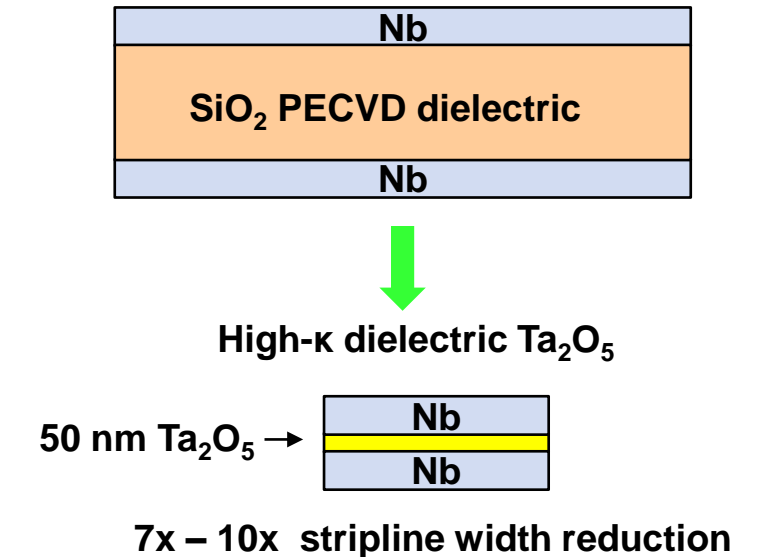
Decrease Area of Circuit Inductors

- Develop kinetic inductors using superconducting NbN and NbTiN thin films instead of Nb geometrical inductors



Decrease Linewidth of Data, Clock, and AC Power Transmission Lines

- Develop high- κ , low-loss interlayer dielectric instead of conventional SiO_2





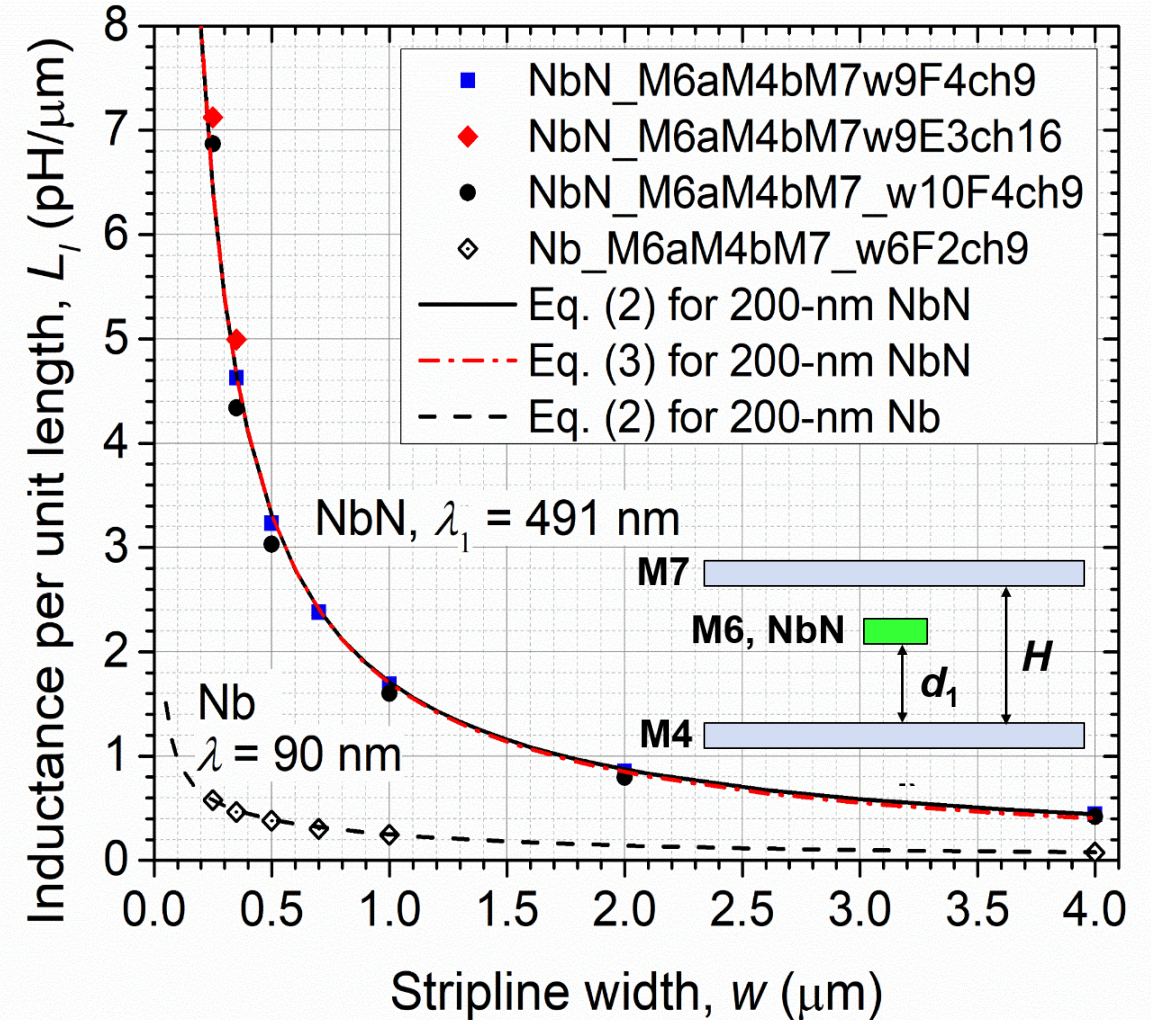
Inductance of NbN (and Nb) Striplines with Nb Ground Planes

$$L_l = \underbrace{\frac{\mu\mu_0}{4\pi} \ln \left(1 + \frac{\sin^2 \frac{\pi \left(d_1 + \frac{t_1}{2} + \lambda \right)}{H + 2\lambda}}{\sinh^2 \frac{0.2235\pi(w+t)}{2(H+2\lambda)}} \right)}_{\text{Geometric Inductance:}} + \underbrace{\frac{\mu_0 \lambda_1^2}{t_1 w}}_{\text{Kinetic Inductance:}}, \quad (3)$$

Geometric Inductance:
dominates for Nb
 $\lambda \sim 90$ nm

Kinetic Inductance:
dominates for NbN
 $\lambda \sim 490$ nm

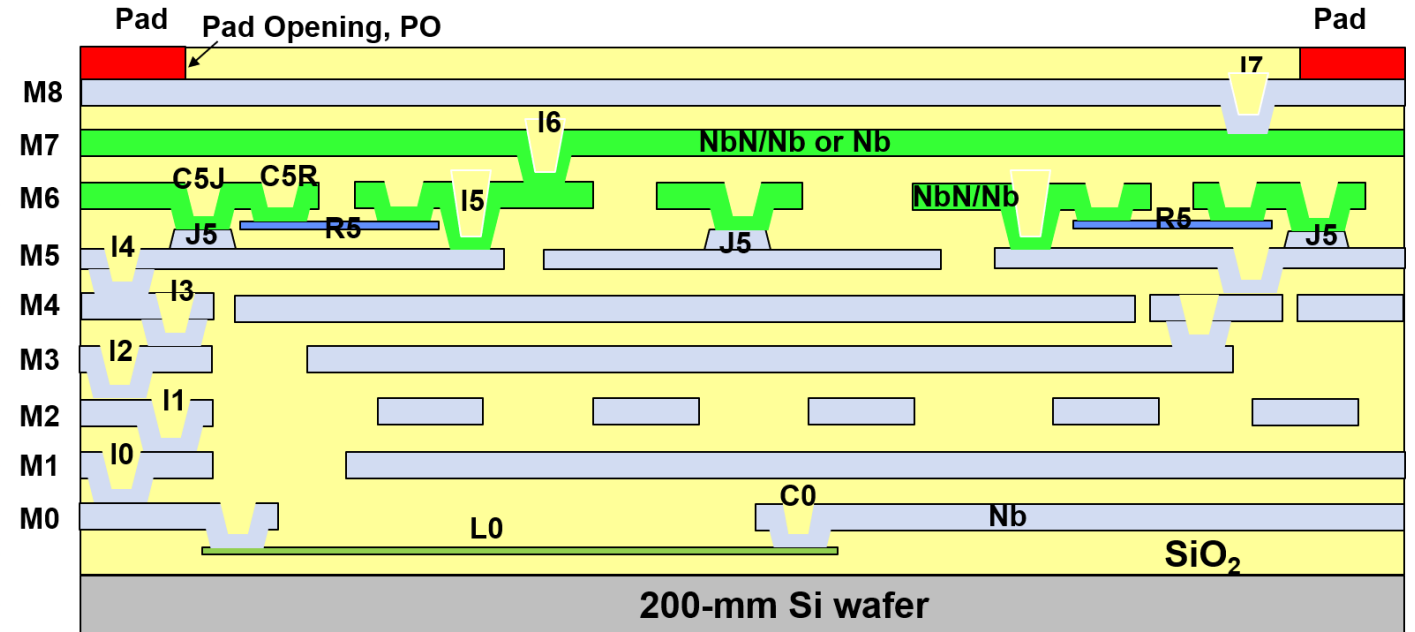
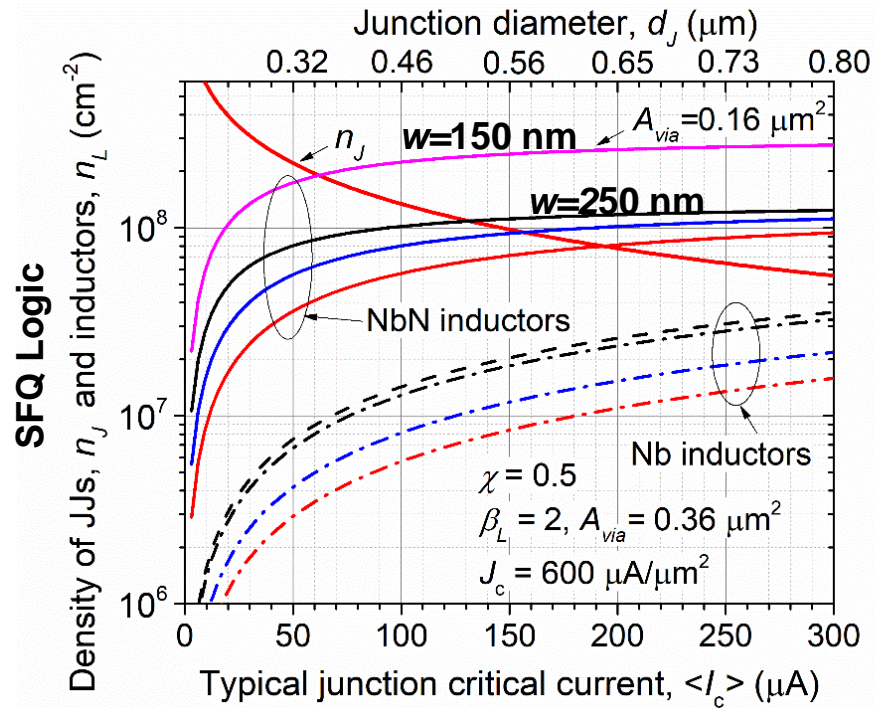
- Excellent agreement between measurements and model
- Determined NbN kinetic inductance: $L_K = 1.51$ pH/sq





SFQ7ee Process

SFQ Logic

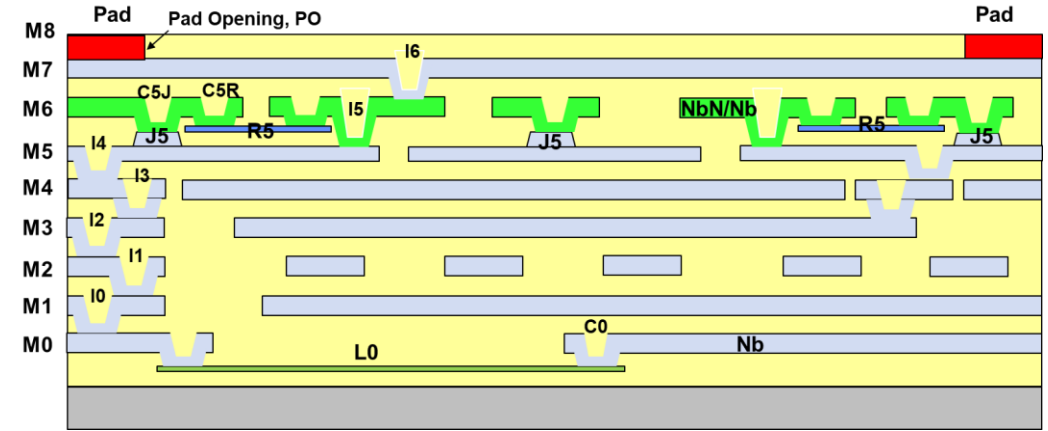


- **Balancing number densities of self-shunted Josephson junctions and inductors requires compact kinetic inductors**
- **Circuit densities $\sim 100\text{M}$ JJs per cm^2 are achievable in the SFQ7ee process**
 - Target $J_c = 600\ \mu\text{A}/\mu\text{m}^2$, self-shunted, $d = 400\text{ nm}$
 - One – two layers of kinetic inductors $w = 250\text{ nm}$ for logic, and one layer for bias inductors



Development of Compact Inductors with NbN/Nb Bilayers

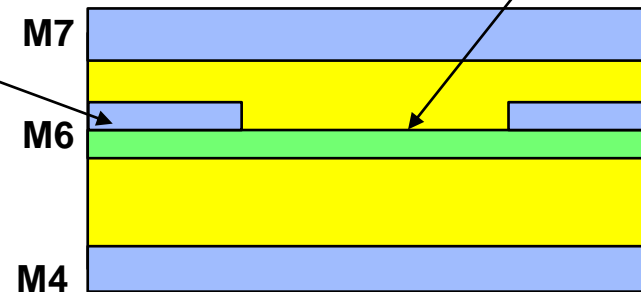
- NbN thin films have high kinetic inductance (resulting from large penetration depth $\lambda \sim 490$ nm)
 - L_{KI} proportional to λ^2/tw
 - Larger than 200-nm film thickness, thus compromising shielding properties
- Developing alternative approach utilizing NbN/Nb bilayers
- NbN-only regions have high kinetic inductance, tunable over wide range up to 30 pH/ μ m
- Bilayer inductance is the same as of 100-nm Nb layer – effective for shielding



Patterned M6 NbN kinetic inductor

NbN/Nb bilayer region inductance dominated by Nb

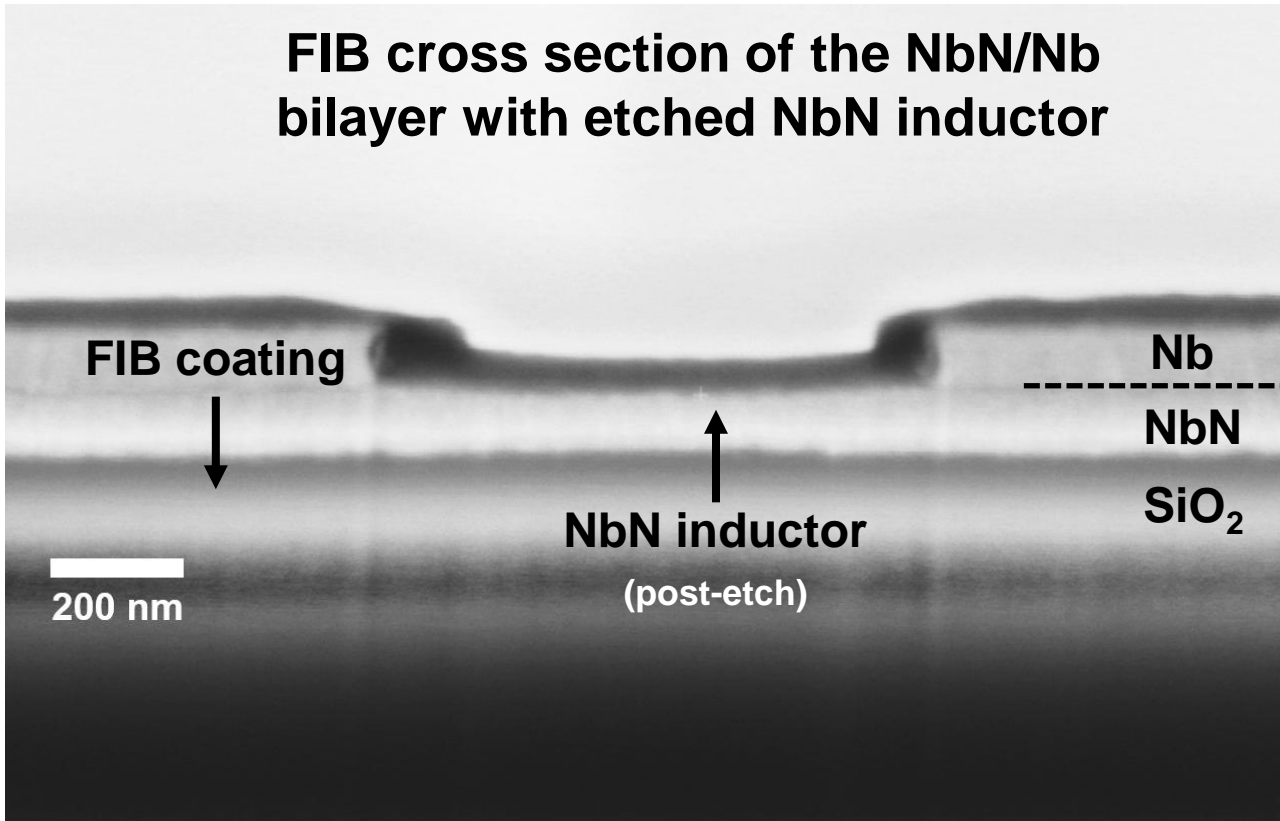
Bilayer behaves electrically as 100-nm-thick Nb layer at 4 K



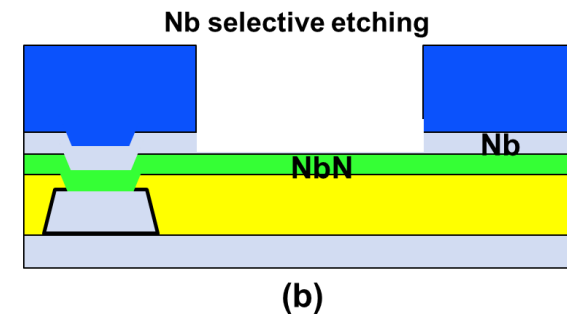
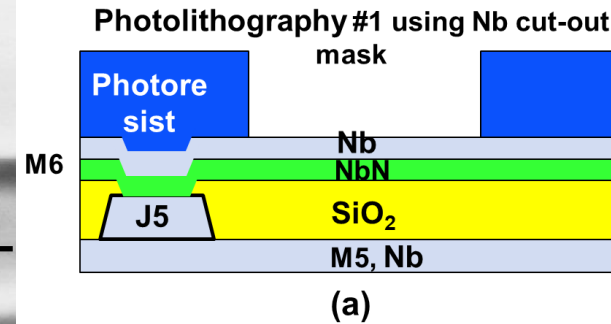
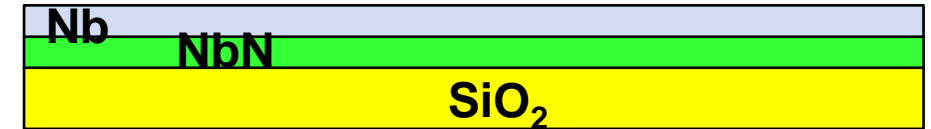


Bi-Layers for Circuit Inductors and Transformers

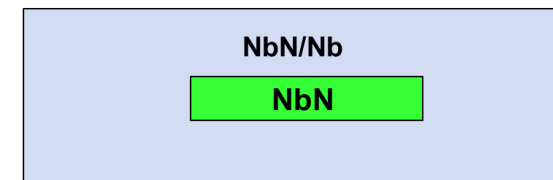
FIB cross section of the NbN/Nb bilayer with etched NbN inductor



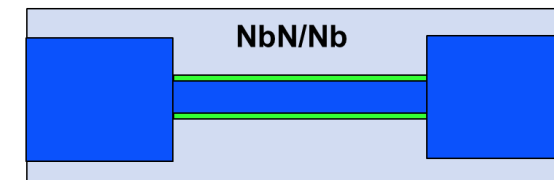
NbN/Nb bilayers as inductor layers



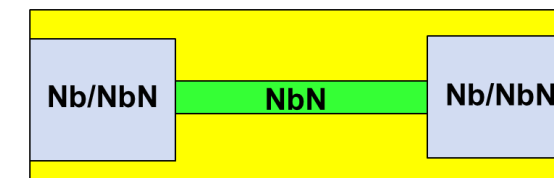
Top view after etching



Photolithography #2, top view



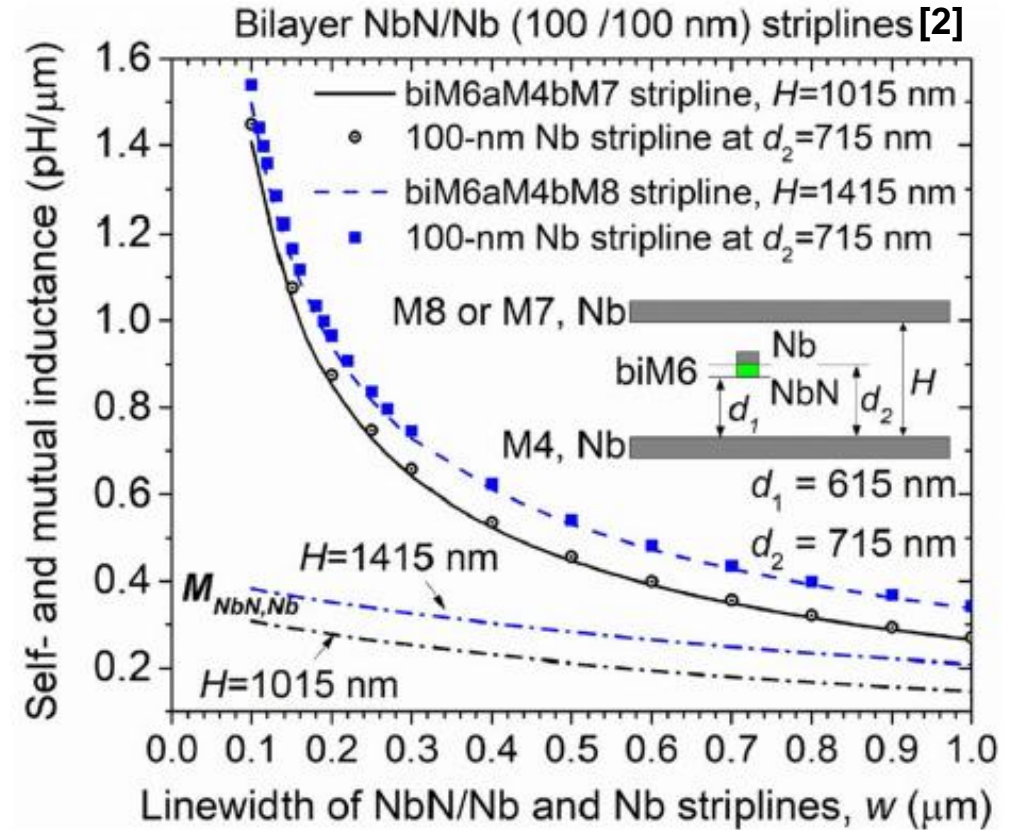
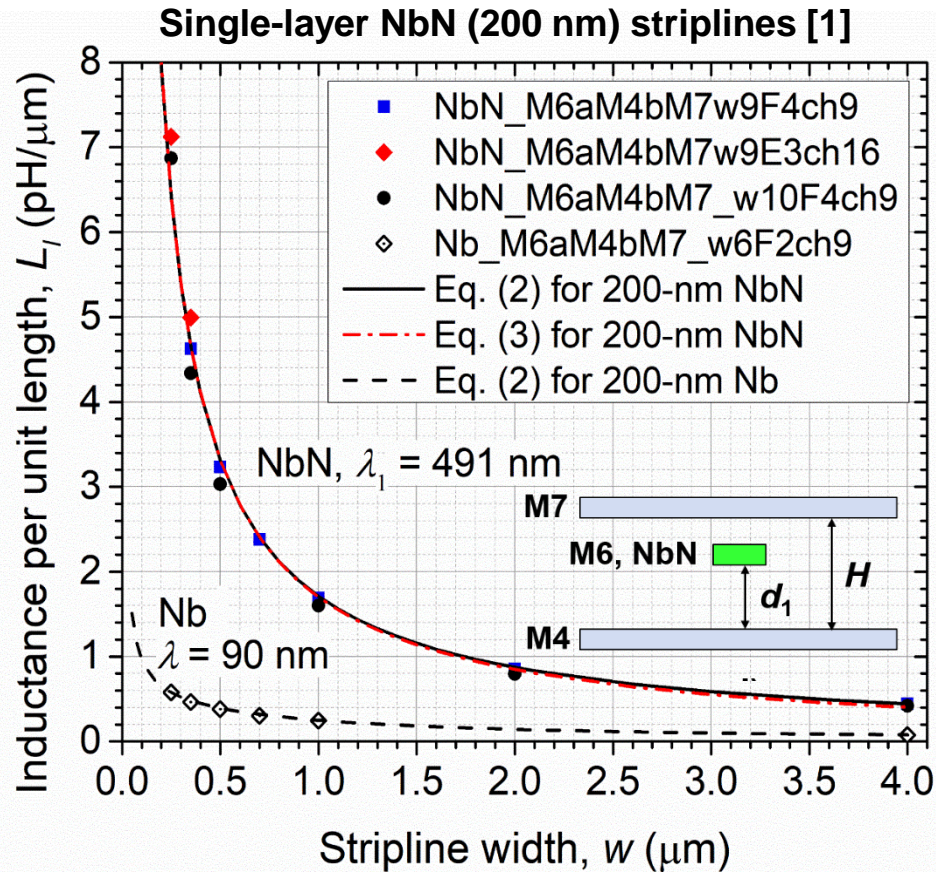
After bilayer etching and resist strip



(e)



Single-Layer & Bilayer Stripline Inductors



Bilayer (NbN/Nb) striplines dominated by Nb geometric inductance (as expected)

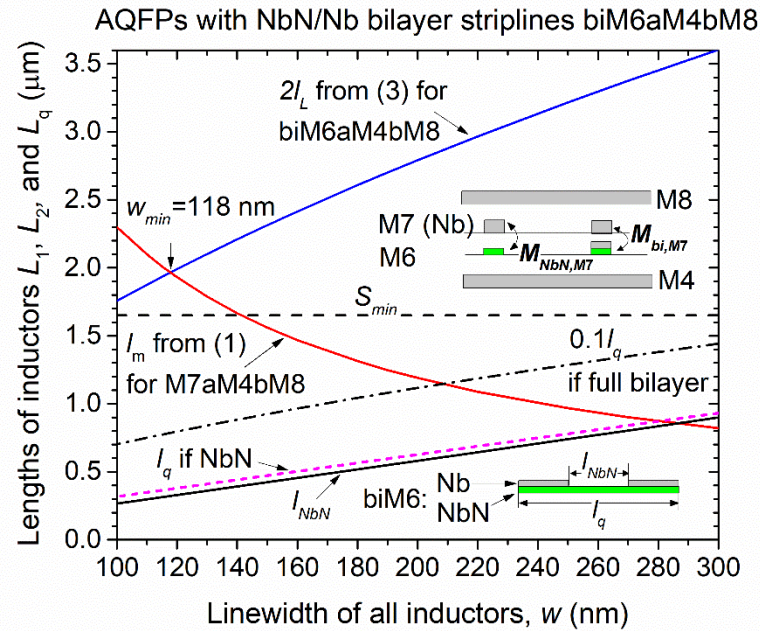
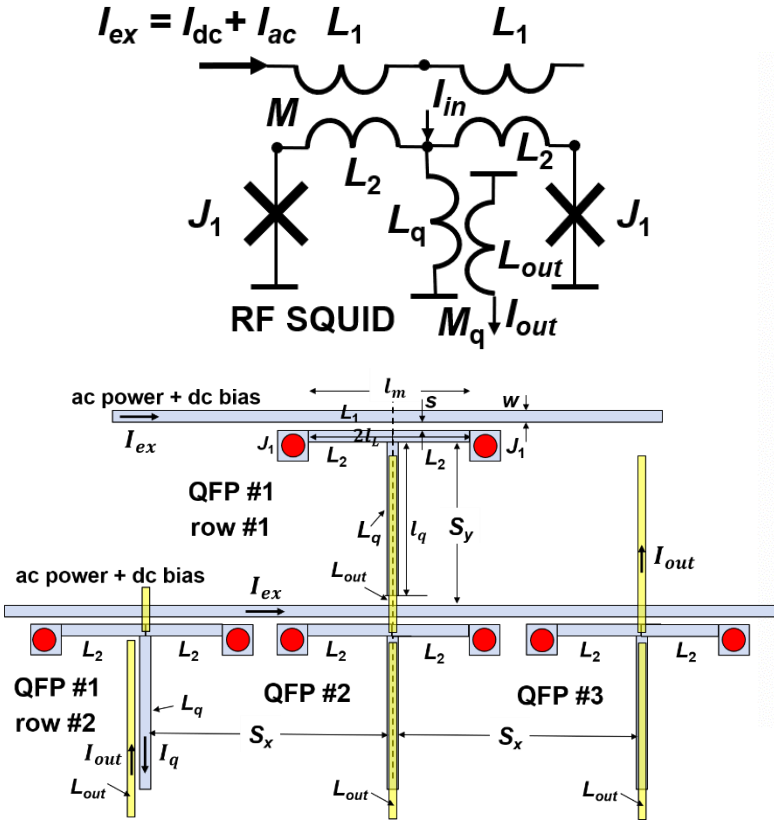
[1] Tolpygo et al., *IEEE Trans. Appl. Supercond.*, 33 (Article # 1101911) (2023)

[2] Tolpygo, *IEEE Trans. Appl. Supercond.*, 33 (Article # 1300419) (2023)



AQFP Scaling in SFQ7ee & Beyond

Parameters of ac excitation transformer, AQFP cell inductors (Nb & NbN striplines)

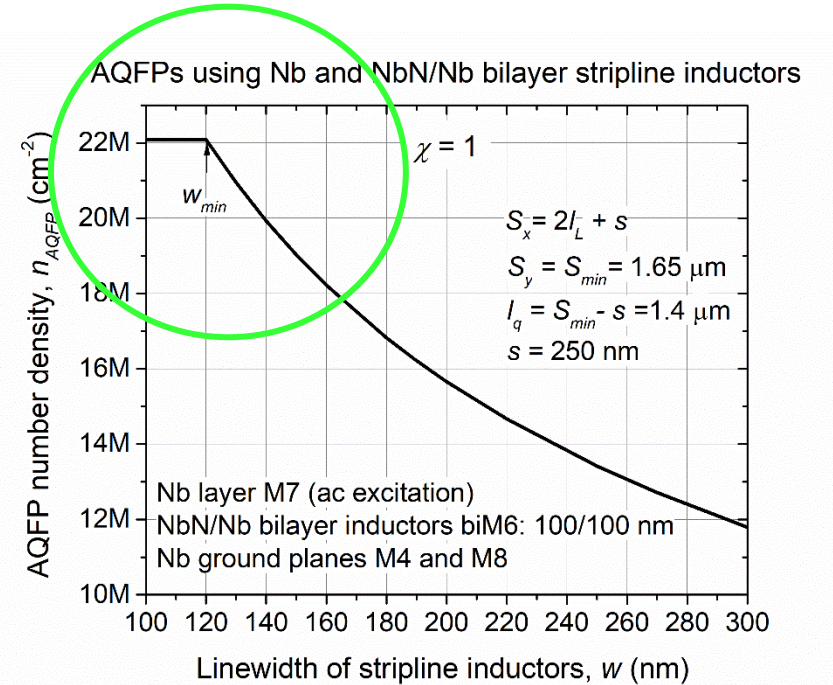


$$\beta_L = \frac{2\pi I_{CJ} L_2}{\Phi_0} = 0.2$$

$$\beta_q = \frac{2\pi I_{CJ} L_q}{\Phi_0} = 1.6$$

$$J_c = 100 \mu\text{A}/\mu\text{m}^2$$

$$I_{CJ} = 50 \mu\text{A}$$

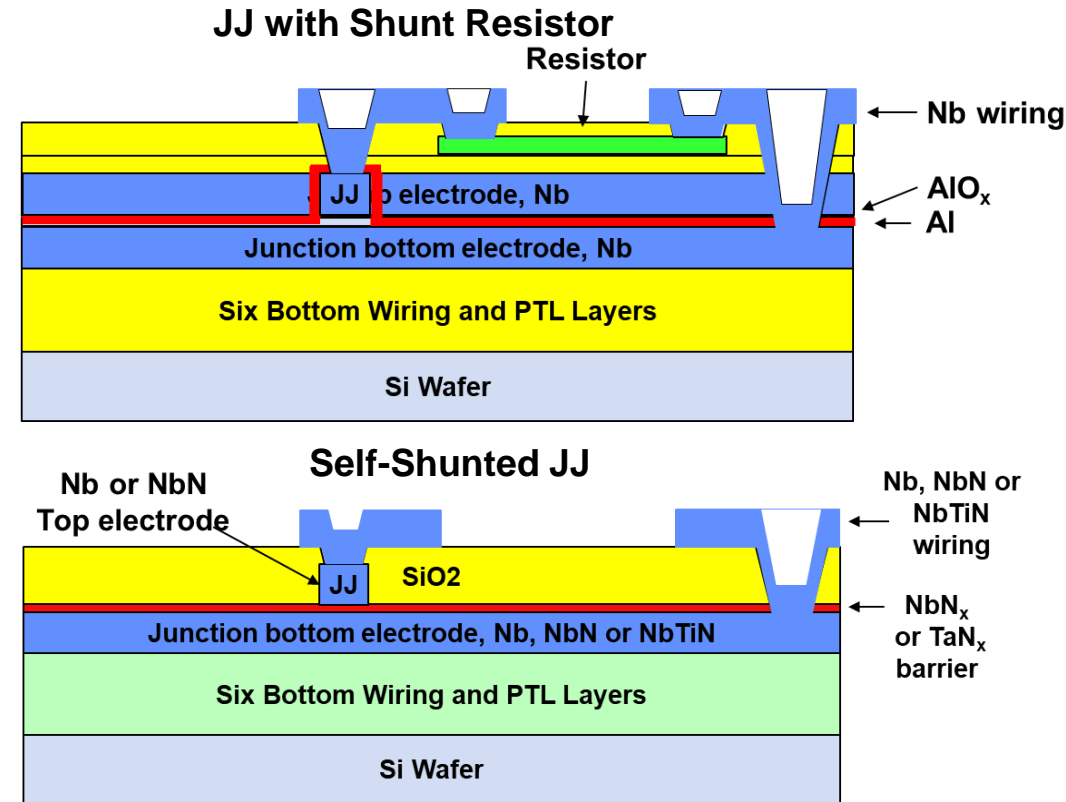
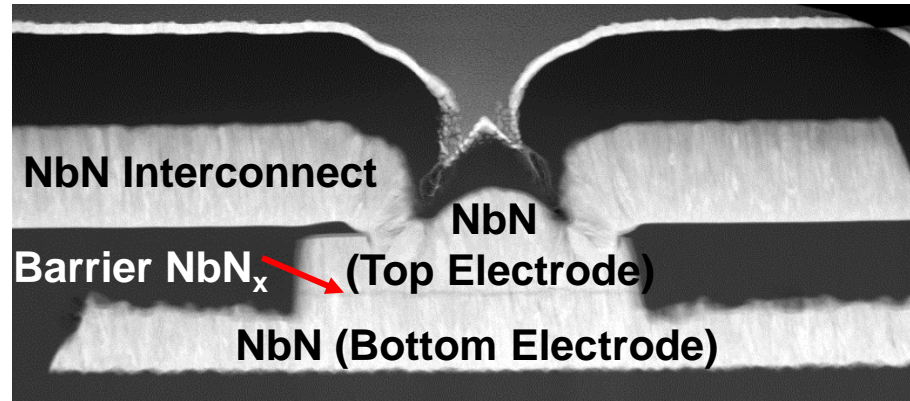
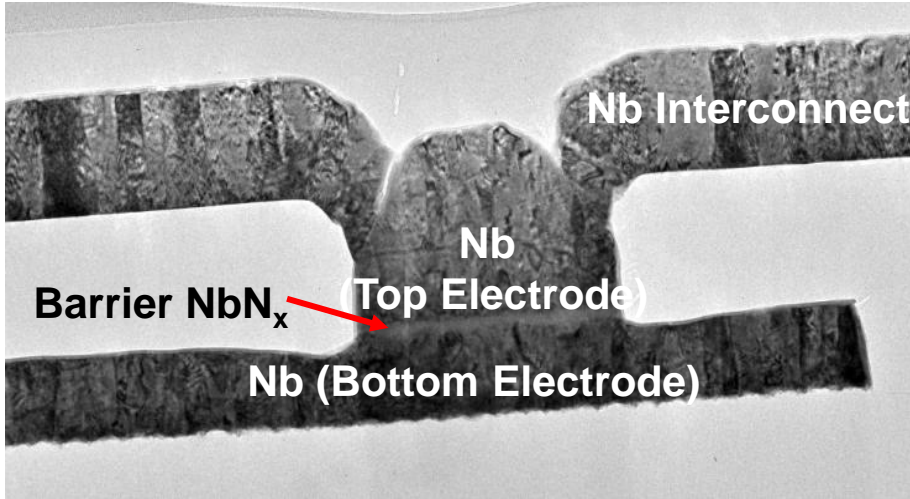


Path to ~20M AQFPs/cm² with advanced process node



Development of SNS Self-Shunted Josephson Junctions

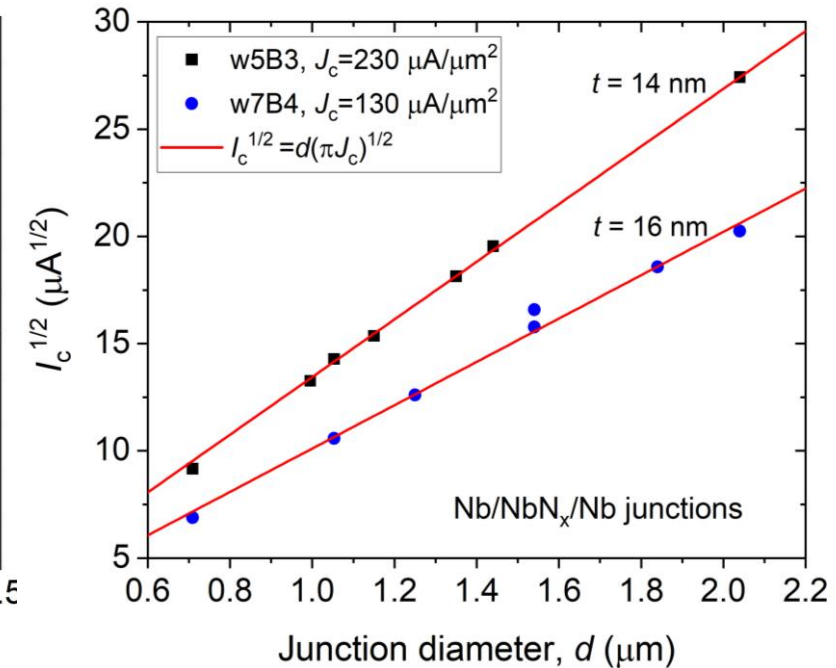
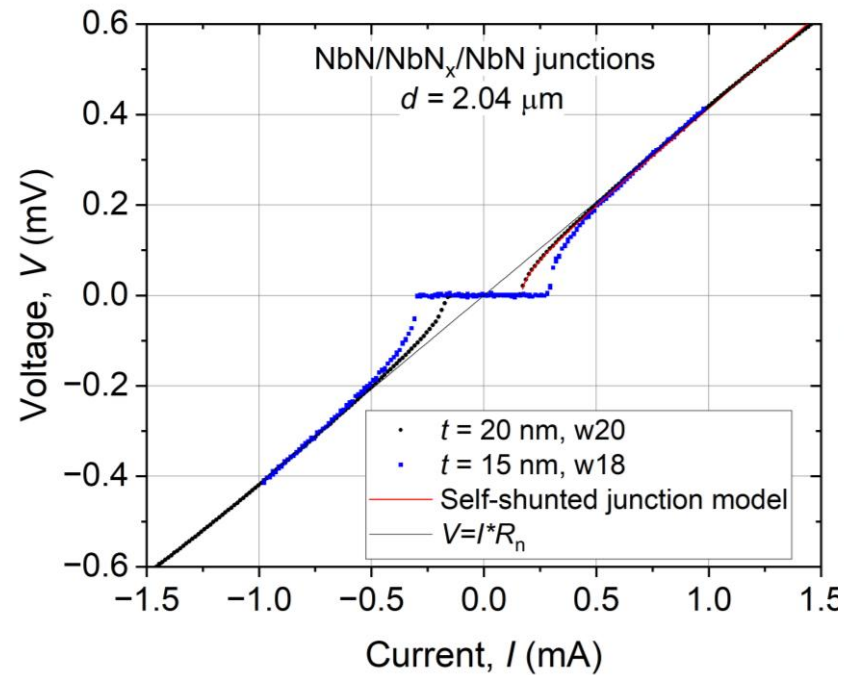
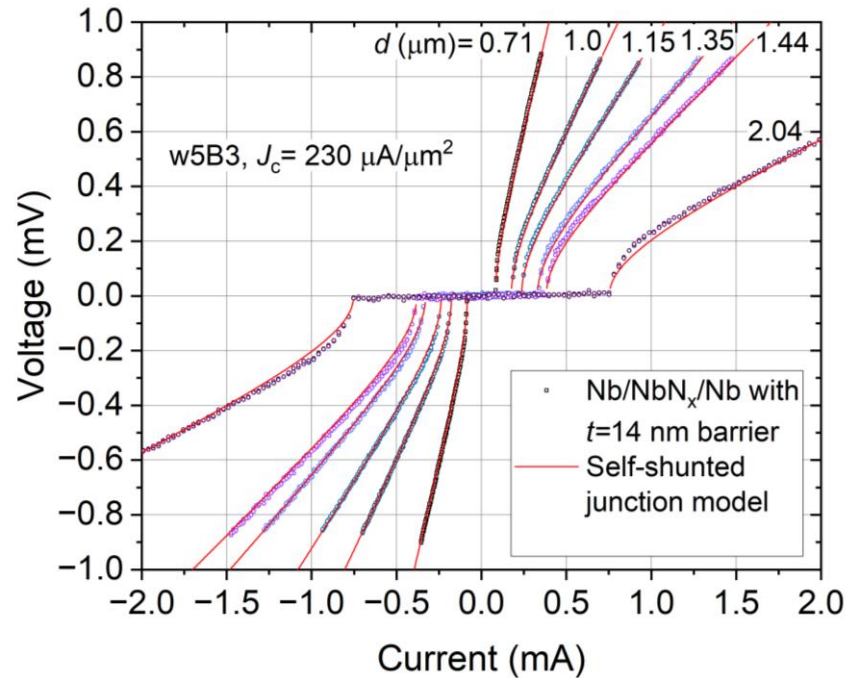
TEM Cross-section of the fabricated devices



- Nb/Al-AIO_x/Nb tunnel junctions are used as active devices in SCE
 - These JJs are hysteretic and require resistive shunting to remove hysteresis
 - Shunt resistor increases the device area by about 10x
- Replaced 1-nm AIO_x barrier with 5-10 nm high-resistivity NbN_x or TaN_x to obtain self-shunted JJs with the same critical current density (J_c)



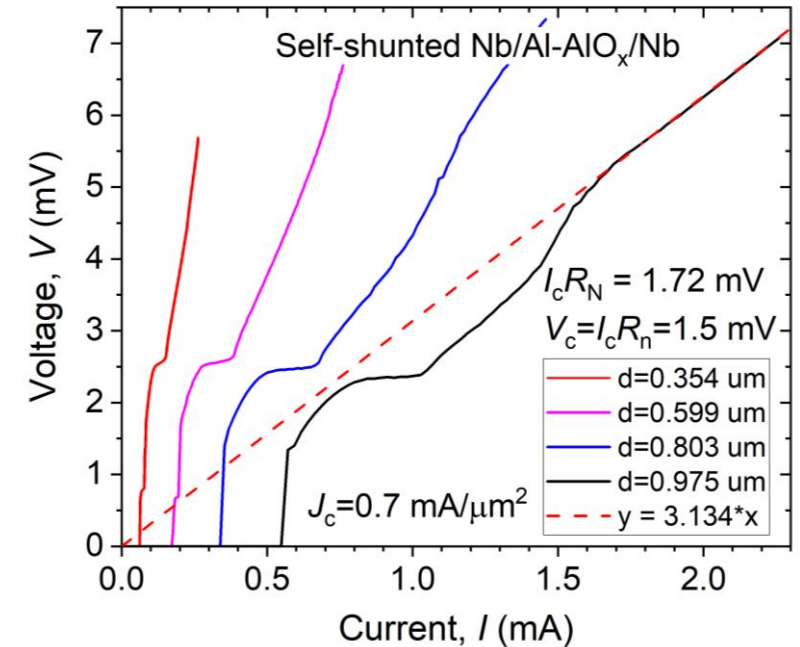
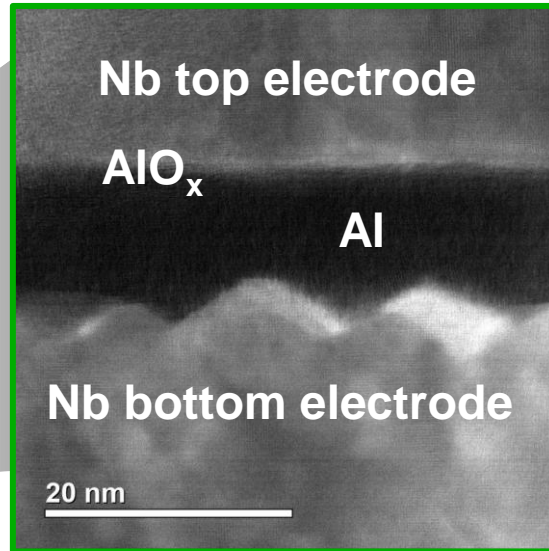
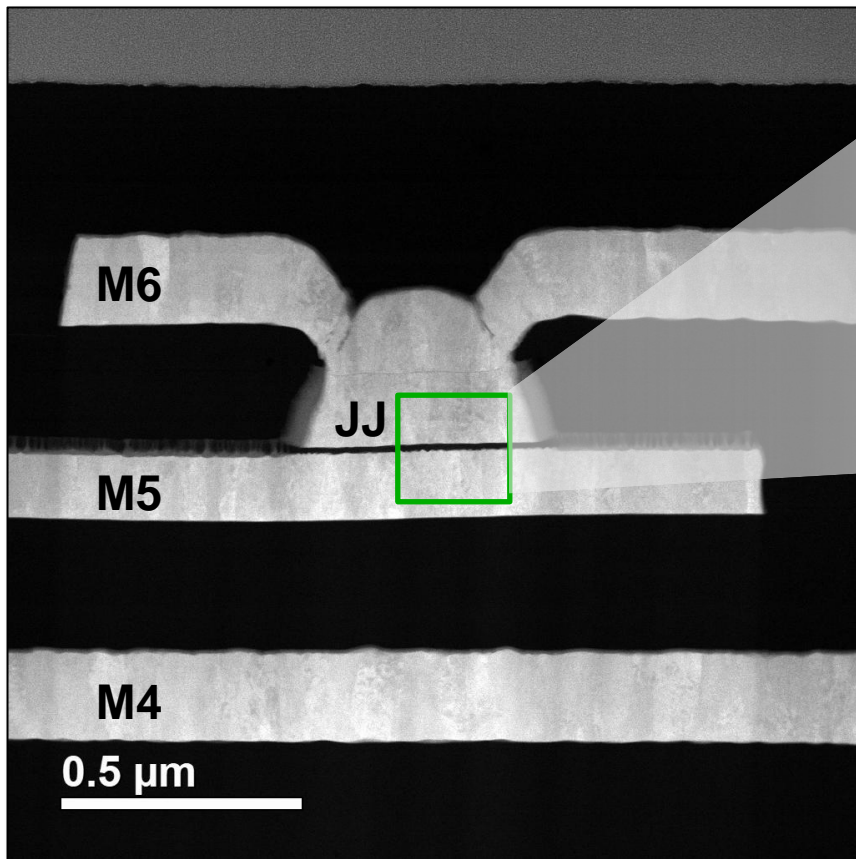
Electrical Properties of Nb/NbN_x/Nb and NbN/NbN_x/NbN Josephson Junctions



- I - V characteristics show no hysteresis and are very well described by a self-shunted (intrinsically shunted) junction model
- Critical current of the junctions properly scales with the junction area, $I_c \propto A \Rightarrow \sqrt{I_c} \propto d$



AlO_x -Based Self-Shunted JJs



- **Self-shunted AlO_x -barrier JJs are more difficult to fab because J_c is**
 - sensitive to film stress and roughness in Nb bottom and top electrode
 - sensitive to Al thickness, roughness, and granularity
- **However, Nb/Al- AlO_x /Nb JJs have a 4x – 5x larger $V_c = I_c R_n$ than JJs with deposited disordered barriers (NbN_x, TaN_x, doped a-Si,...)**
- **Much weaker critical current temperature dependence $I_c(T)$; better across wafer J_c uniformity**



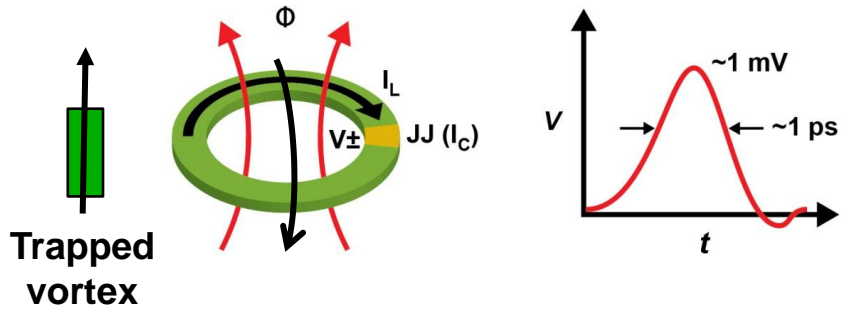
Outline

- **Overview of MIT Lincoln Laboratory SCE integrated circuit foundry**
- **SCE digital logic applications and motivation for advanced process nodes**
 - In context of continuing advances in digital CMOS technology
- **Advanced process node development (SFQ7ee)**
 - **Emphasis on increasing SCE circuit density**
 - Compact kinetic inductors
 - Self-shunted Josephson junctions
- ➔ • **Flux-trapping diagnostics and mitigation**

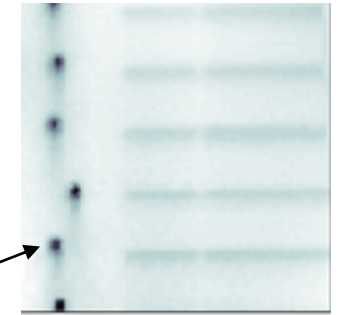
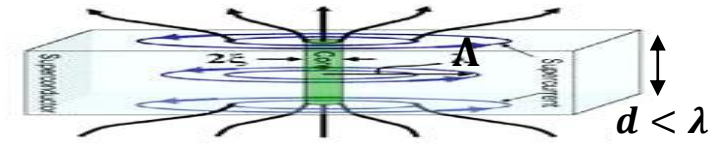


Superconducting Digital Logic Flux Trapping

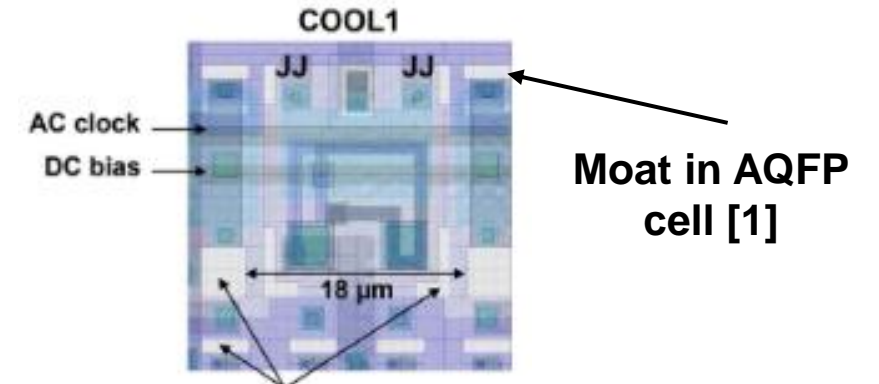
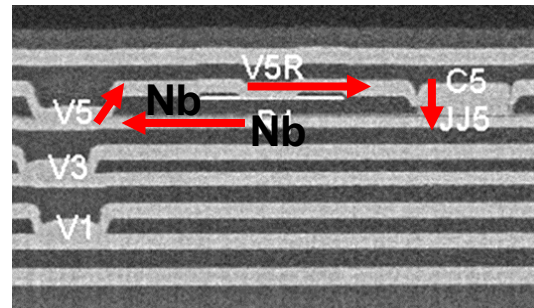
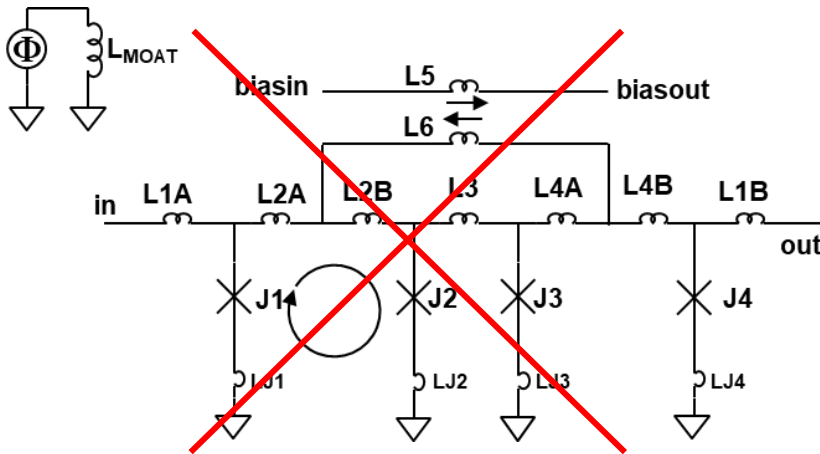
Superconducting loop



Pearl vortex



Flux trapped in film



Moats in M4 ground plane
Fluxon trapped in moat produces a much smaller magnetic field than a vortex in the film

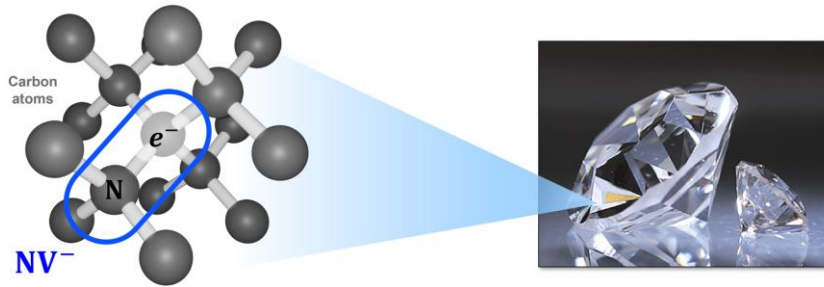
Trapped flux can adversely affect SFQ circuit operation: need effective mitigation techniques



QSWIFT: Magnetic Microscopy for SDL Diagnostics

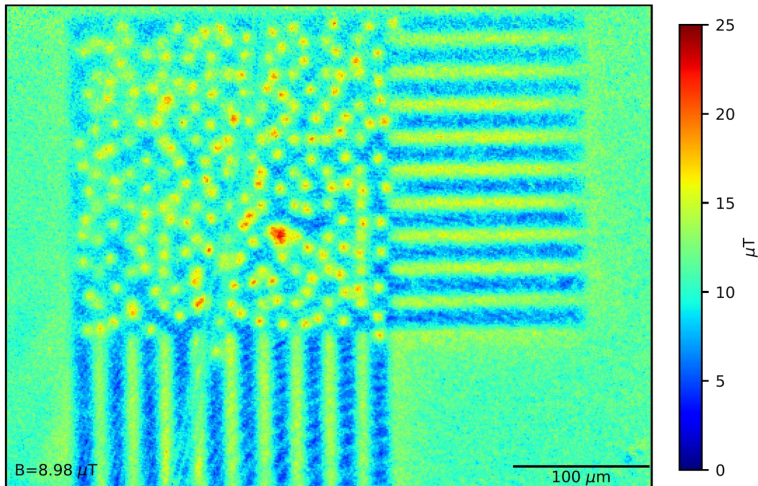
Quantum Solid-state Widefield Imager of Flux Trapping

Diamond Nitrogen-Vacancy (NV) Centers Sense Magnetic Fields



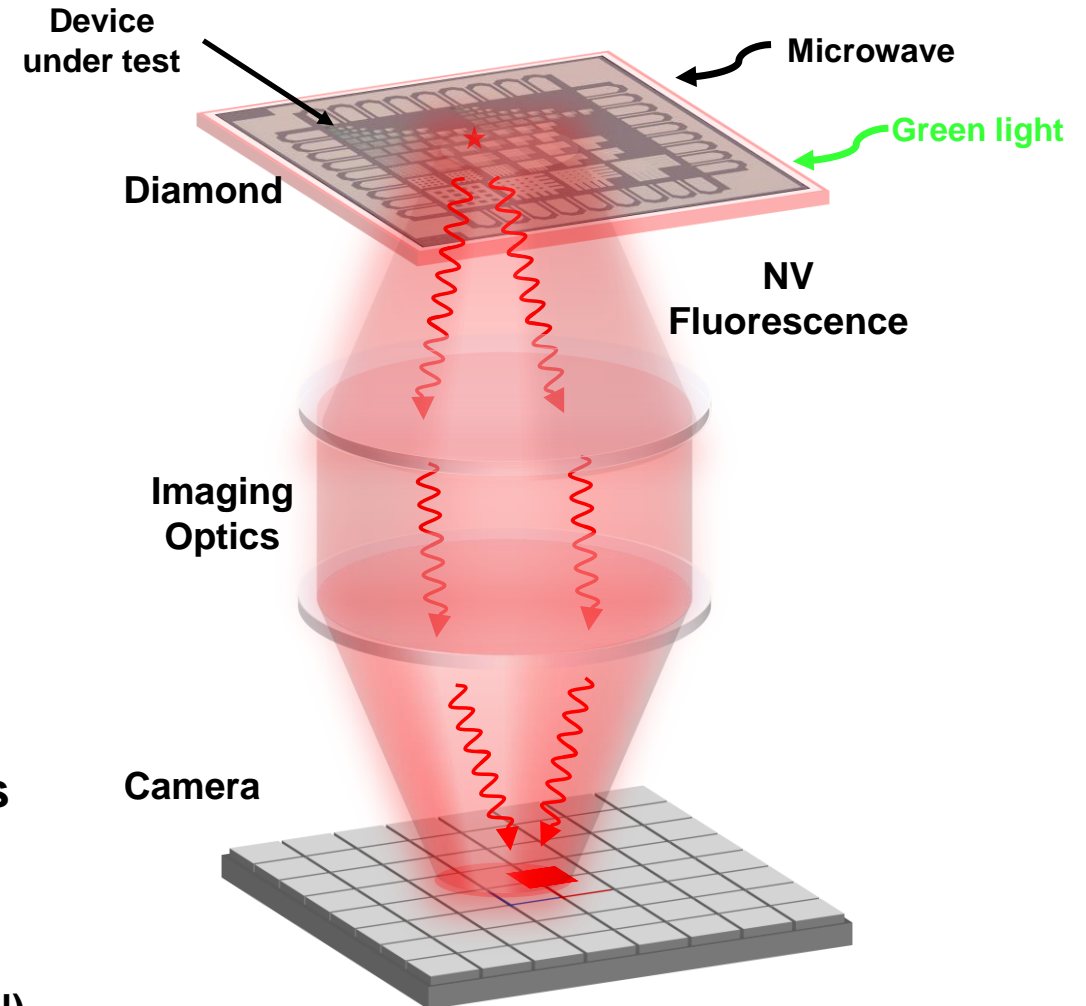
QSWIFT Magnetic Image of Trapped Flux in Superconducting Test Structure

Magnetic Field in $20\ \mu\text{m}$ Strips, Below Critical Field



- Fast, global imaging
- Micron-scale resolution
- Repeated measurements across T_c

See arXiv:2506.01906 (Kapur et al)





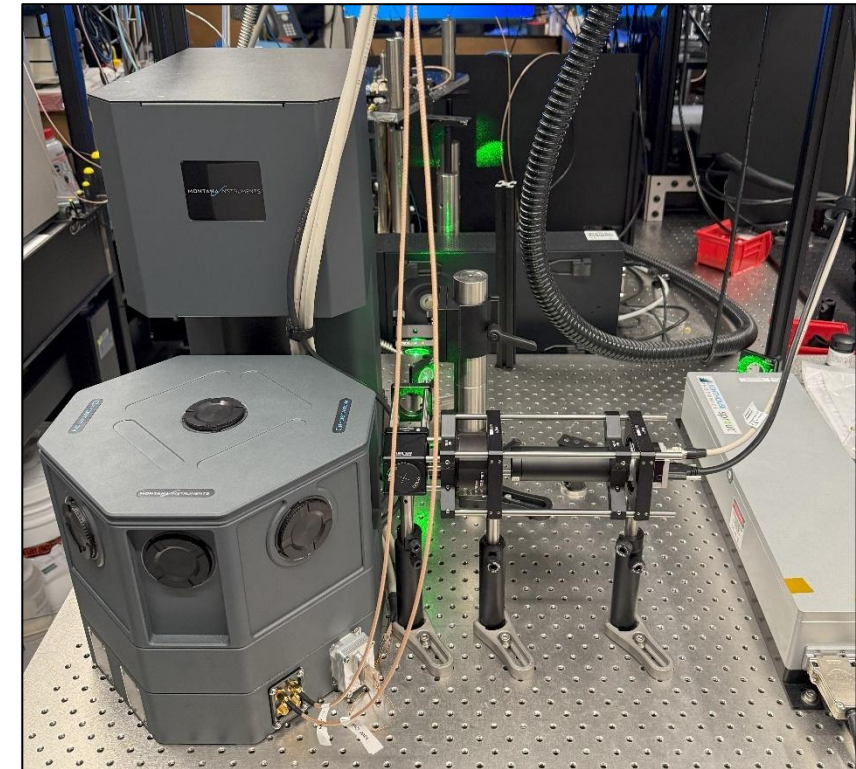
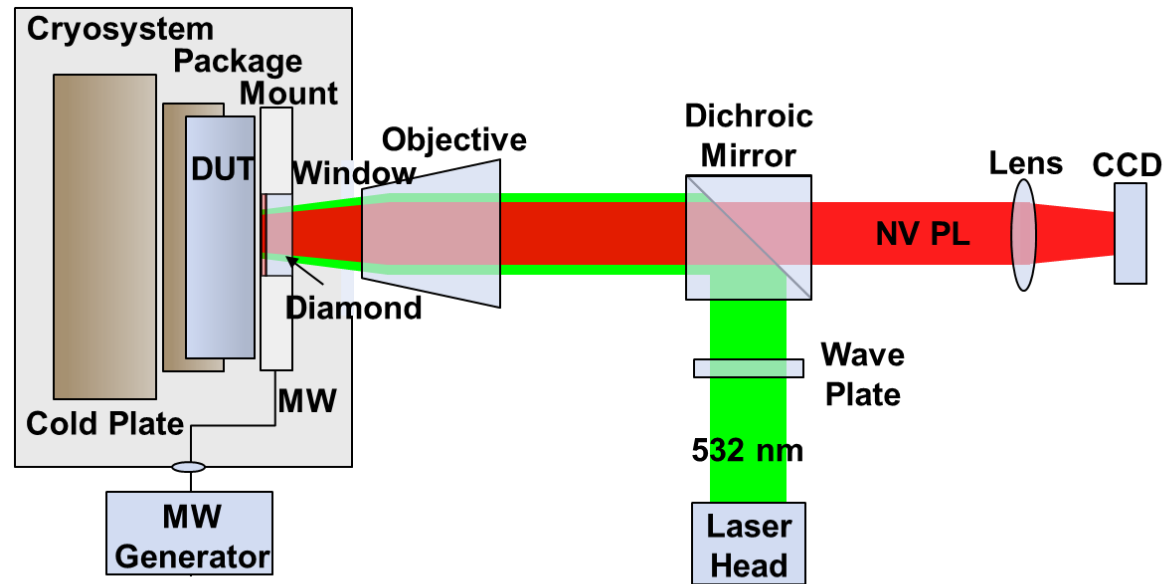
Magnetic Imager Comparison

	NV Widefield Microscope	Magneto-Optic Imaging (MOI)	NV Scanning Tip (NV-AFM)	Scanning SQUID	Scanning Hall Probe
Spatiotemporal Dynamics	Global Imager	Global Imager	Raster Scan	Raster Scan	Raster Scan
Typical field of view (FOV)	500 × 500 μm ²	50 × 50 μm ²	20 × 20 μm ²	200 × 200 μm ²	100 × 100 μm ²
Spatial Resolution	Few-μm	Few-μm	Tens of nm	~100 nm	Few-μm
Sensitivity					
Time to measure 1 × 1 mm²	Tens of seconds to minutes	Seconds to minutes	Hours	Tens of minutes to hours	Hours
Comments	Opportunities to improve sensitivity, resolution, & FOV	Incompatible with many applications, usually qualitative	Best for small-area scans	Limited by scan speed	Limited by scan speed



QSWIFT Architecture

Widefield magnetic imager purpose-designed for flux trapping diagnostics



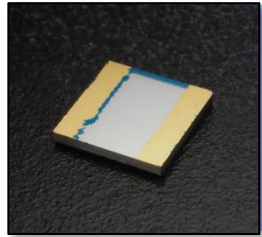
QSWIFT: Quantum Solid-state Widefield Imager of Flux Trapping



QSWIFT Architecture

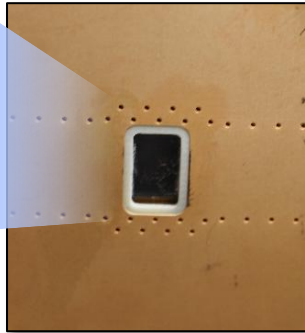


NV Diamond



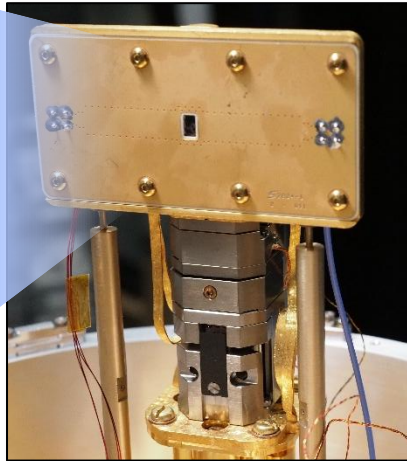
Tailored production & custom coatings

Diamond Stackup



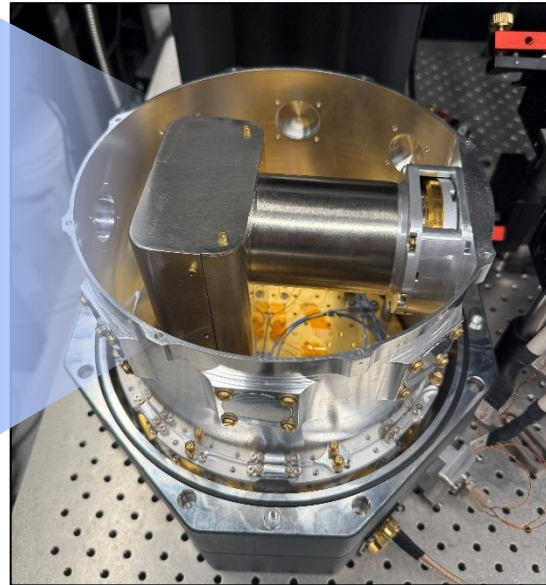
EM shielding, microwave delivery, & sample interfacing

Sensor Head



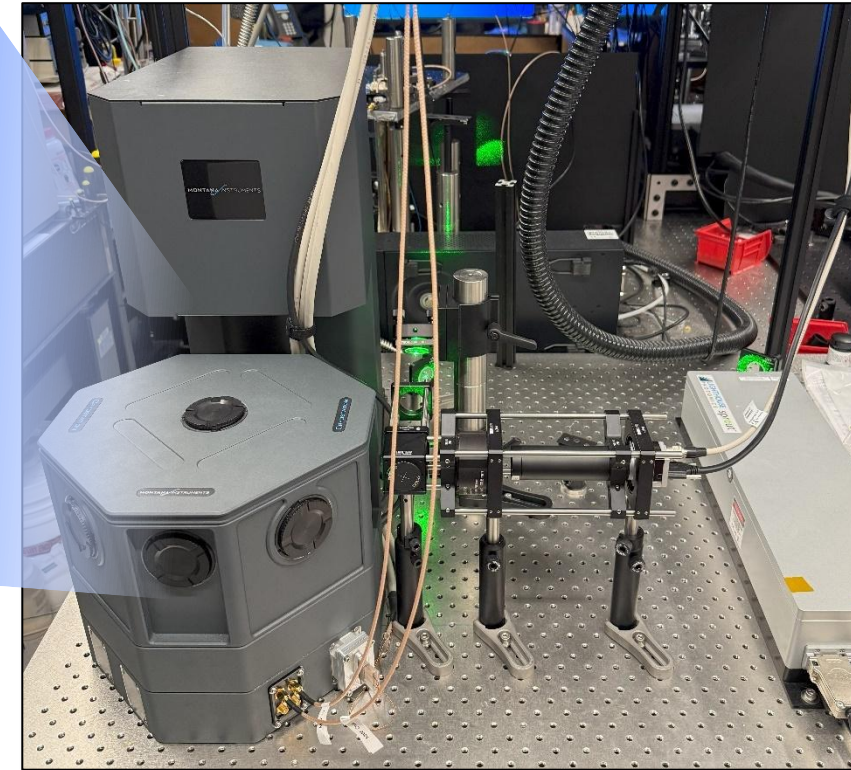
Thermal management, sensors, coils, & translation

Measurement Chamber



Customized cryostat & custom magnetic shielding

QSWIFT Cryomicroscope System



Optical microscope and system control outside cryostat

↑
Sample isolation from laser light

↑
Micron-scale proximity to sample

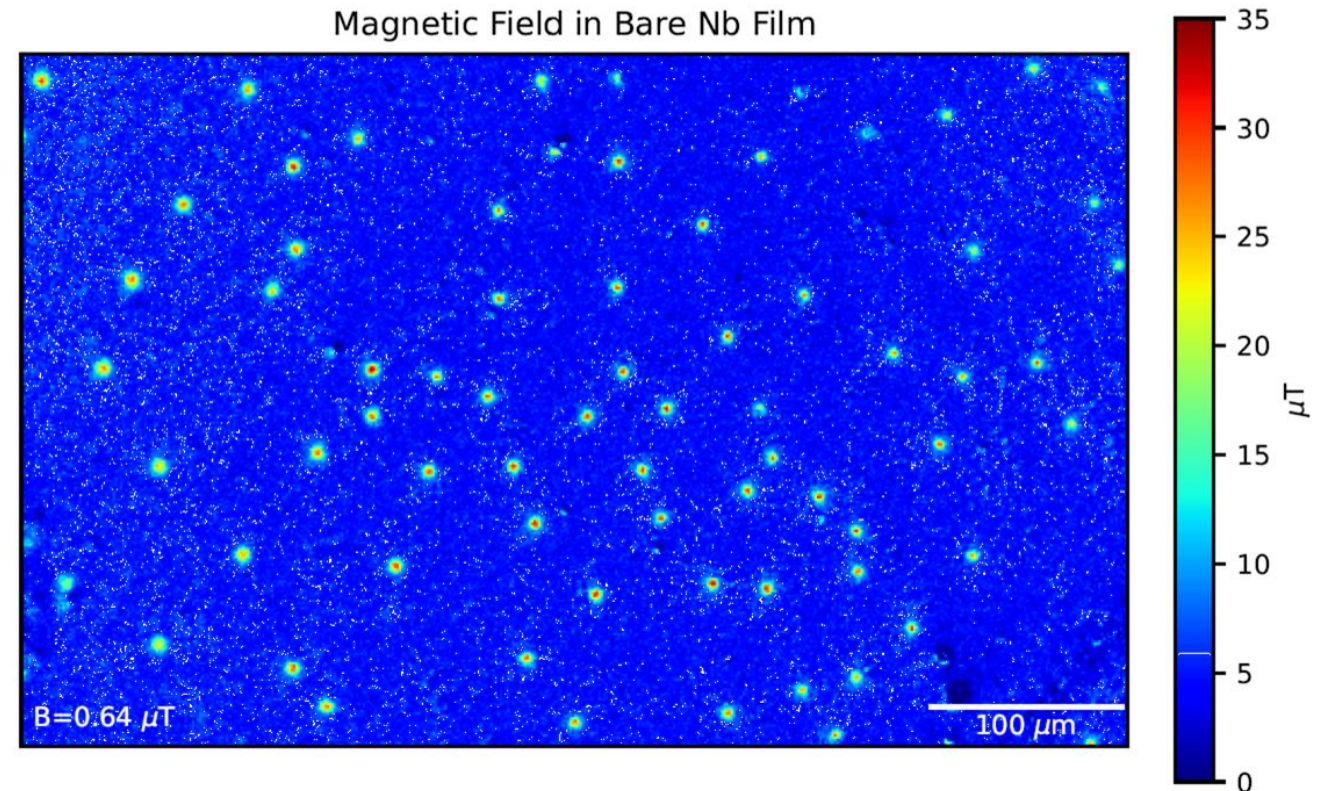
↑
10 nT background magnetic field

↑
4 K operation (<T_c of niobium)



Imaging Vortices in a Bare Niobium Film

- **Vortices visualized in 200nm Nb film**
 - High SNR in minutes per image
 - Few-micron resolution
 - 580 x 360 μm^2 , tileable field of view

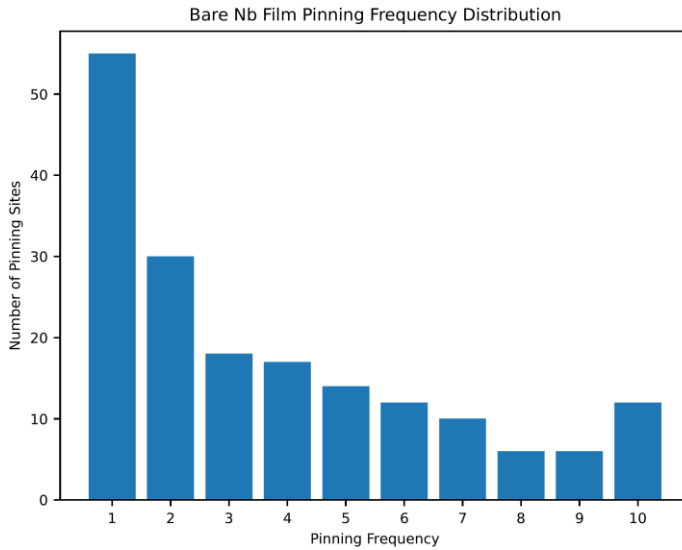
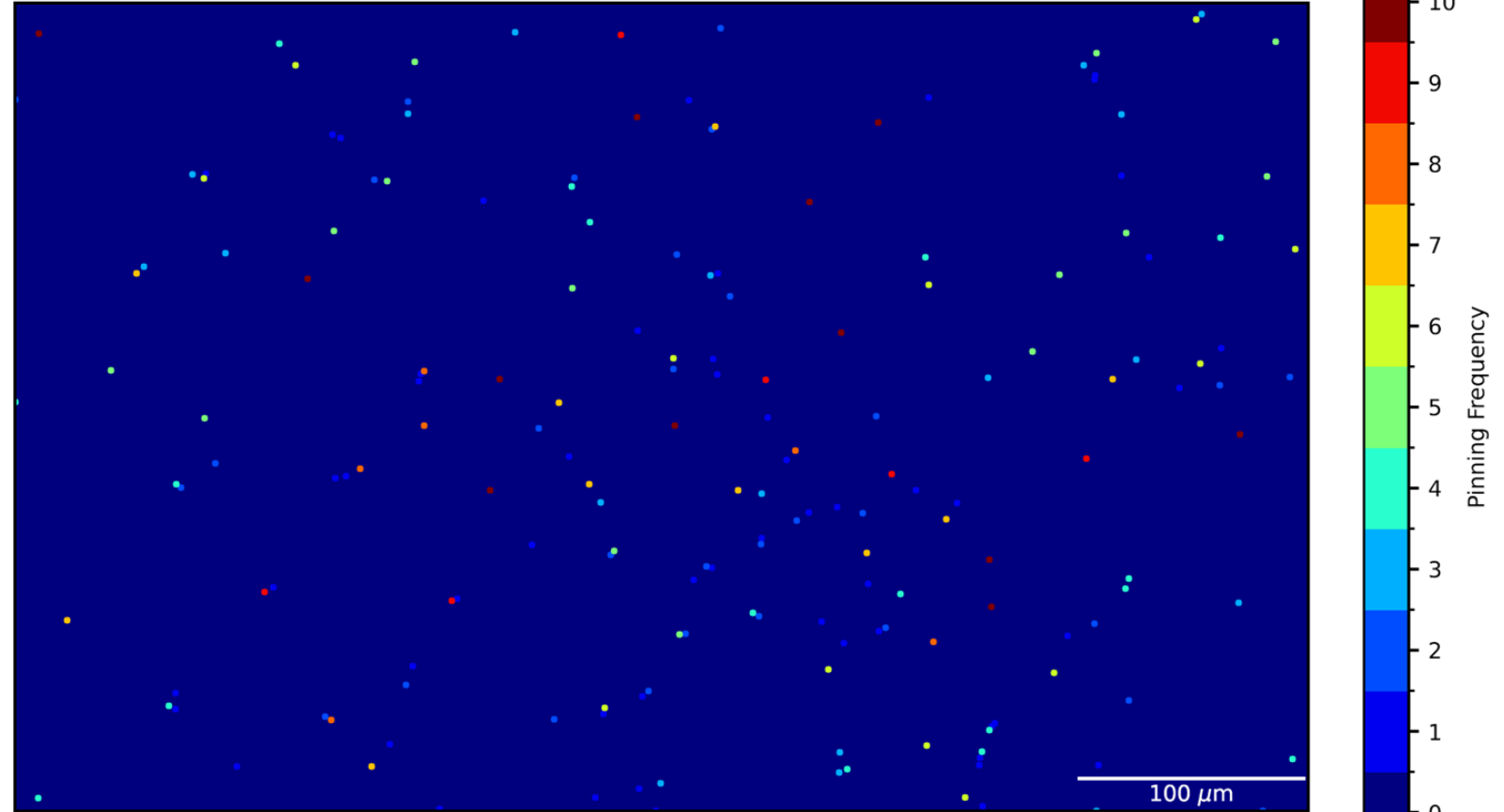




Preferential Flux Pinning in Nb Film

Vortex statistics upon 10 cooldown cycles through T_c

Bare Nb Film Flux Pinning Sites



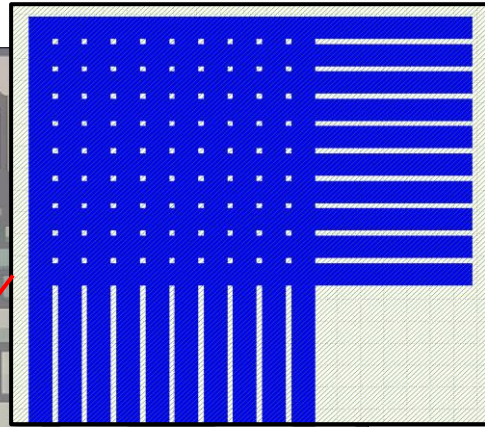
A majority of sites are observed to pin vortices multiple times

Pinning locations considered discrete when separated by $>1.5 \mu\text{m}$

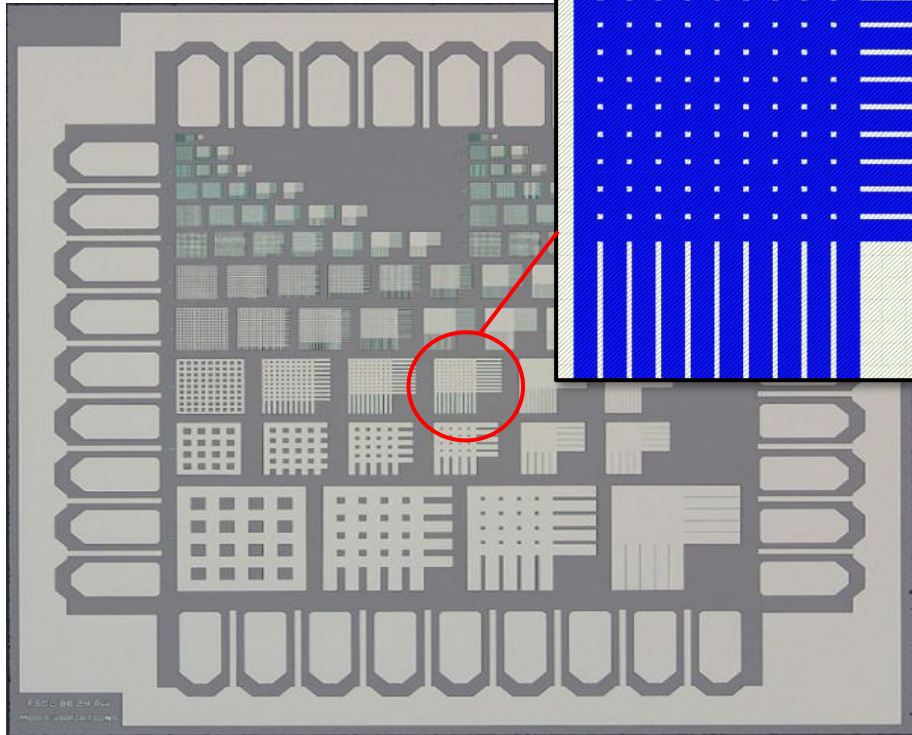
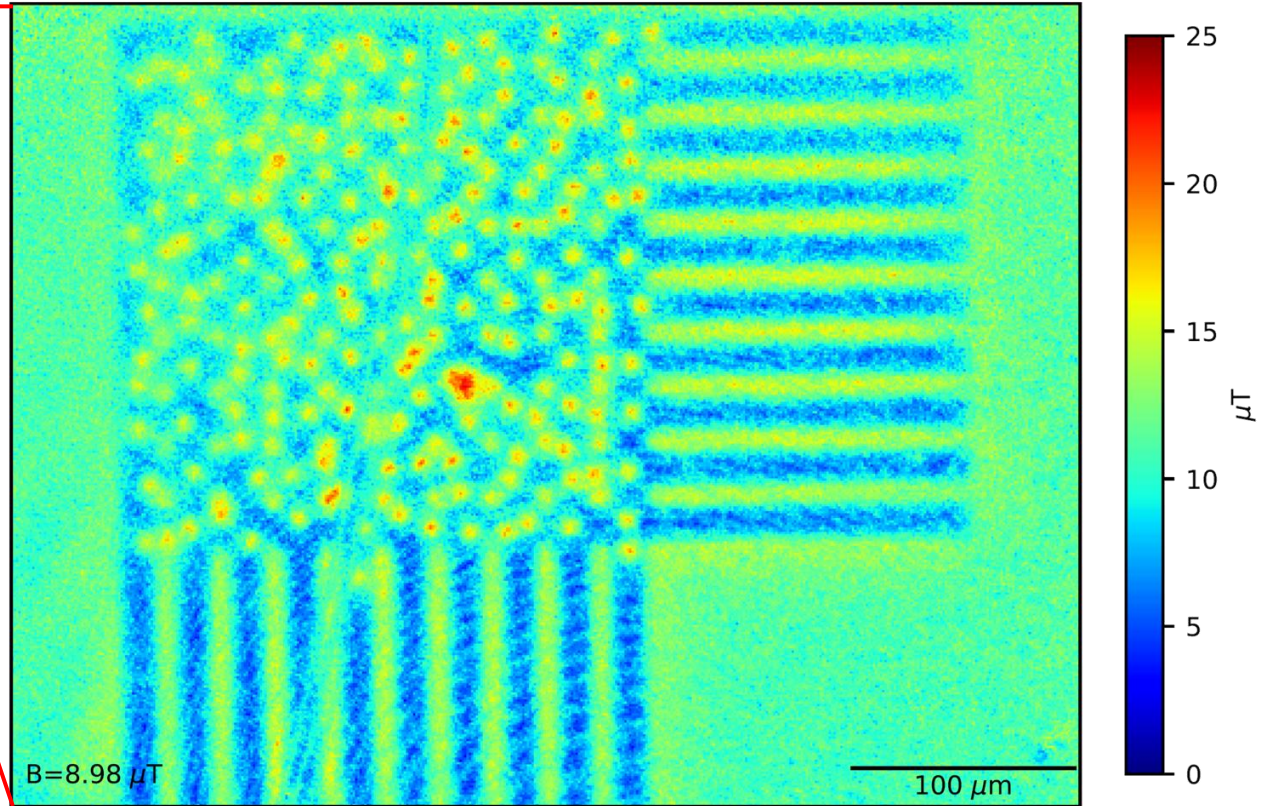


Field Expulsion in Intersecting Strips and Moats

Intersecting 20 μm Strips



Magnetic Image Below Critical Field of Strips



FOCuS Intersecting Strip Array Test Chip

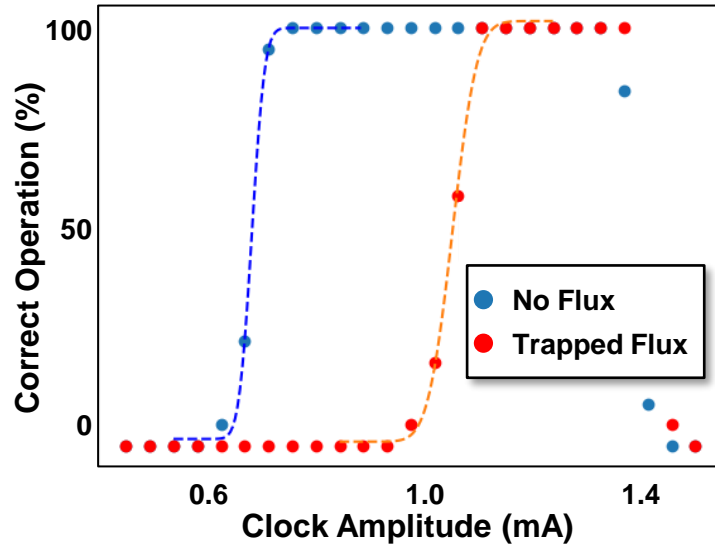
>20x lower critical expulsion field in intersecting regions than in strips

Early indication that flux trapping in 2D circuits does not follow intuition based on 1D systems

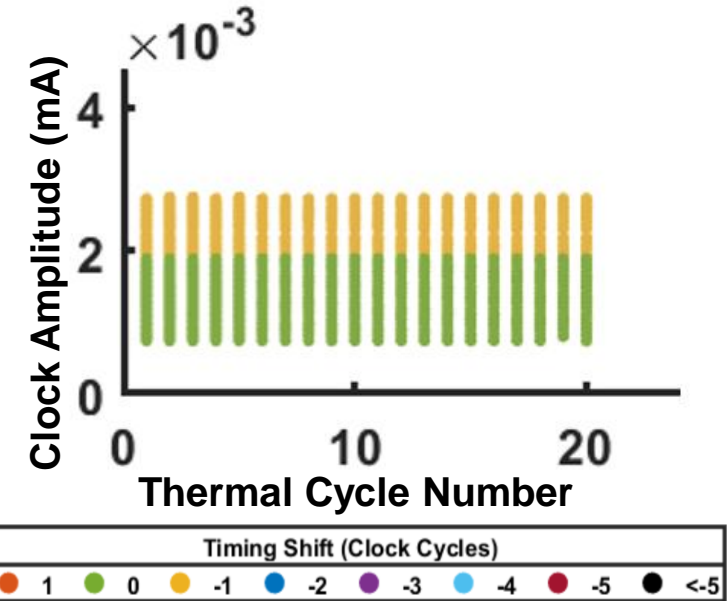
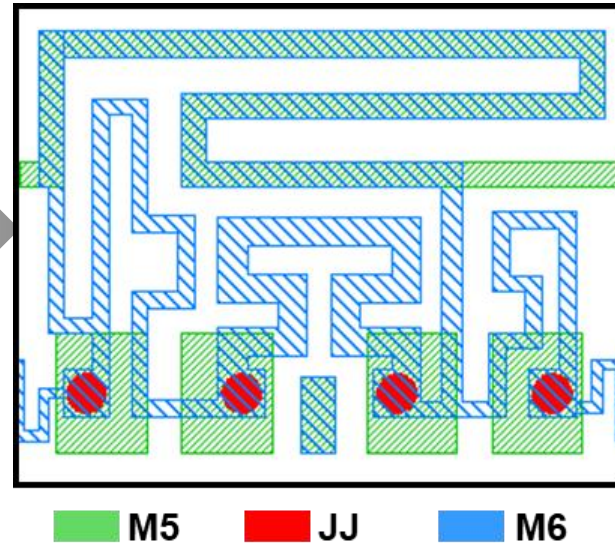


Flux Observation Control and Sequestration (FOCuS)

Circuit Simulation



Design



Integrate flux simulations into circuit design workflows

Design and fabricate benchmark circuits to study flux trapping

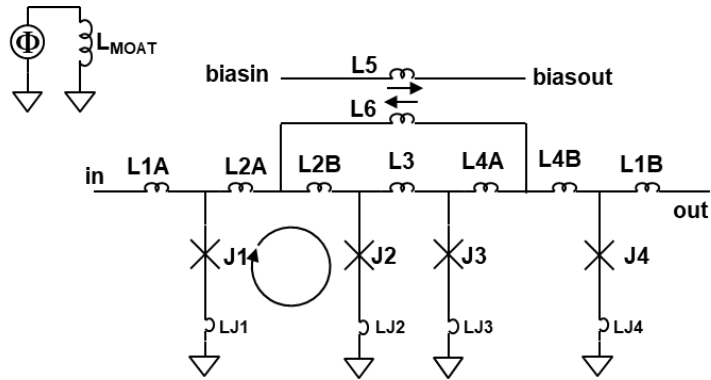
Perform in-house electrical testing to verify simulation results

MIT LL is working toward a foundational understanding of flux trapping in superconducting digital logic circuits

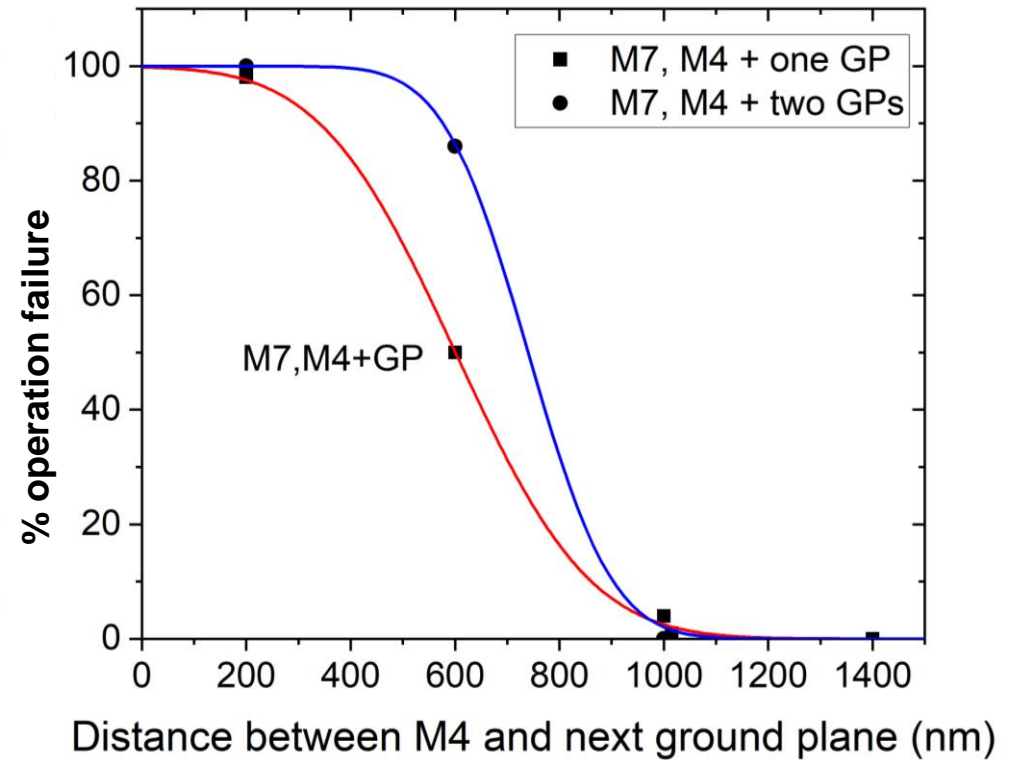
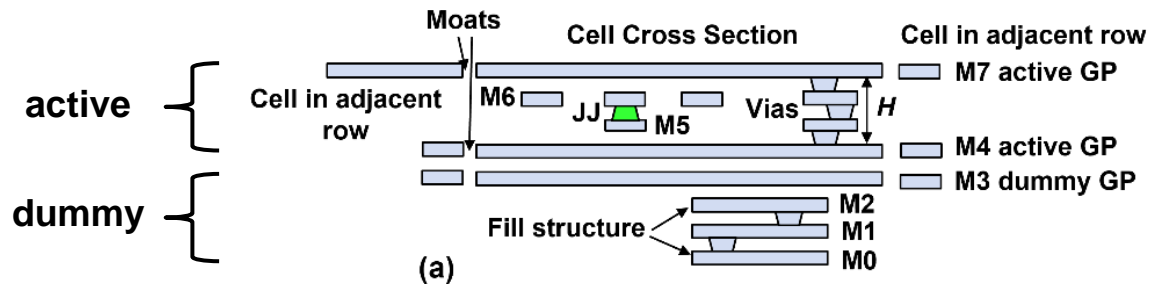


Effect of Multiple Ground Planes on Flux Trapping

Flux-shuttle shift register



Single 'dummy' ground plane



Closely spaced GPs can strongly enhance detrimental flux trapping outside moats



Summary

- **Superconducting electronics provides a combination of higher speed and lower energy dissipation exceeding that of any other beyond-CMOS digital logic integrated circuit technology**
- **Increasing circuit density (gates per cm^2) enables future applications**
- **Both compact (kinetic) inductors and self-shunted Josephson junctions are key elements of advanced process nodes**
- **Continuing progress in evaluating and mitigating causes and effects of flux trapping in SCE integrated circuits**



Acknowledgements

Quantum-Enabled Computation Group



Group Leaders: Mollie Schwartz, Jonilyn Yoder, Joe Belarge, Julie Haiar, Kyle Serniak, Steven Weber

Senior Staff: Jeffrey Birenbaum, A. Jamie Kerman, Lenny Johnson, Kevin Obenland, Sergey Tolpygo

Group: James Aguilar, Kate Azar, Peter Baldo, Anthony Bishop, Logan Bishop-Van Horn, Maria Blood, Tristan Brown, Luke Burkhart, Gregory Calusine, Glenn Carl, Lynn Clifford, Felipe Contipelli, John Cummings Jr, David Danza, Rabindra Das, Daniel Davis, Renee DePencier Pinero, Steve Disseler, Justin Elenewski, Ben Freiman, Jeffrey Gertler, Michael Gingras, Evan Golden, David Goldfinger, Ben Goodwin, Kevin Grossklaus, Karen Harmon, Thomas Hazard, Michael Hellstrom, Cyrus Hirjibehedin, Gerard Holland, Jennifer Hritz, Bethany Huffman, Sokharom Huon, Erin M. Jones-Ravgiala, David Kim, Jeffrey Knecht, Parker Kukulinski, Arthur Kurlej, Shavonne LaFauci, Justin Mallek, Andrew McKie, Roderick McNeill, Scott Menger, Duncan Miller, Nathan Miller, Jovi Miloshi, Maddie Morocco, Kaitlyn Morrell, Zain Mughal, Rylee Neumann, Chris O'Connell, Neel Parmar, Susan Pitman, Maria Prado Rodriguez, Mallika Randeria, Ravi Rastogi, Benjamin Rempfer, Matt Ricci, Lila Rodgers, Rob Rood, David Russo, Gabriel Samach, Andrew Savage, Meghan Schuldt, Arjan Sevi, Arnav Sharma, Marcus Sherwin, Katrina Sliwa, Basil Smitham, Hannah Stickler, Manz Thompson, Chris Thourmaraj, Kate Thurmer, Andrew Wagner, Jennifer Wang, Terry Weir, Charles Woodrum, June Woods, Alex Wynn, Donna Yost

MicroElectronics Laboratory



Group Leaders: Dan Pulver, Carrie Huguenin

Group: Mike Antos, Christine Baker, Fredda Bauer, Creda Beauchamp, Susan Bengtson, Matt Blago, Heather Brum, Anne Cappucci, Mark Carroll, Curtis Castello, Brandon Chea, Kevin Checkosky, Vanndy Chhuon, Matt Cook, Jeff DeCaprio, Aishik Dhori, Phil Dimitroglou, Kathy Doan, Charly Em, Timmy Em, Howie Gallant, Jim Gallo, Ben Hall-Seelig, Bob Healey, Bob Holden, Craig Hill, Denise Holohan, John Hunt, Charlie Huoth, Sal Ieni, Matthew Jacobs, Rebecca Kelley, Venne Laine, Dilip Mahenthiran, Mitch Makowicz, Paul Makowicz, Joel Maldonado, Stephen Margiotta, Matt McClellan, James McNaney, Brian Mulloney, Lindina Nith, Samuel Ogura, Nick Oum, John Pentoleros, Penny Phengsavath, Segundo Pichardo, Gianni Pinelli, Alistair Plotnick, Chris Porter, Joe Powers, Angel Reinold, Nazeem Saddeek, George Scetta, Chris Segni, Dmitri Shapiro, Rowan Smith, Bob St. Martin, John Stegner, Jim Stilian, Robin Vitale, Chris Weinburg, TJ Wlodarczak, John Wong, Zallay Yun, Scott Zarr

